HEAT TRANSFER TO FLOWING GRANULAR MEDIA

Thesis by

William Noel Sullivan

In Partial Fulfillment of the Requirements

for the Degree of

Doctor of Philosophy

California Institute of Technology

Pasadena, California

1973

(Submitted September 27, 1972)

ACKNOWLEDGMENTS

The author wishes to express his deep appreciation to Professor Rolf Sabersky for his guidance, advice and patience during the course of this research. The aid of Mr. Don Laird and Mr. Elmer Szombathy in the design and construction of the experimental equipment is appreciated. Thanks are also due Mrs. Julie Powell for her patient typing of the manuscript.

The research presented in this thesis was sponsored by grants from the National Science Foundation (Grant GK-30524) and the Procter & Gamble Company. The author was supported for three years by a United States Steel Industrial Fellowship. Additional financial support was provided by the National Science Foundation and the Esso Education Foundation. The generosity of these contributors is gratefully acknowledged.

ABSTRACT

The convective heat transfer resulting from a granular flow over a heated surface is investigated. The specific type of flow considered is that in which adjacent material particles are in physical contact. The qualitative features of this type of flow are discussed, and the existing equations of motion are extended. With regard to the equations of motion, an exact solution is shown which has applications concerning the mass flow rate of granular materials through hoppers. The particular heat transfer problem investigated is convection from a flat plate with its long axis parallel to the flow field. An approximate analytical solution, which takes into account the particulate nature of the medium, is developed and experimental measurements obtained. The theory was found to correctly predict the trends of the experimental data. The results indicate that the Nusselt number for this configuration is influenced substantially, under certain conditions, by the non-continuous nature of the medium. A semi-empirical correlation is presented, based on experimental results obtained with four different granular materials.

FIGURE CAPTIONS

Figure 1(a)	Flow of sand (top to bottom) about a 1" diameter cylinder at approximately 2" per second.
Figure 1(b)	Flow of sand (top to bottom) about a 1" diameter cylinder at approximately .2" per second.
Figure 2	Flow of sand (top to bottom) about a 1" length double wedge at approximately 2" per second.
Figure 3(a)-(e)	Development of flow about a cylinder with the sand in an initially dense state.
Figure 4	Converging channel with frictionless walls under the influence of a radial body force.
Figure 5	Efflux velocity as a function of material head above the orifice for the radial body force solution.
Figure 6	Dimensionless efflux velocity for sand ($\delta = 35°$) flowing through conical channels.
Figure 7	Dimensionless efflux velocity for glass beads ($\delta = 22°$) flowing through conical channels.
Figure 8	Dimensionless efflux velocity for sand ($\delta = 35°$) flowing through plane channels.
Figure 9	Dimensionless efflux velocity for glass beads ($\delta = 22°$) flowing through plane channels.
Figure 10	Discrete particle flow past a heated plate.
Figure 11	Typical row of particles in a discrete particle flow.
Figure 12	Dimensionless temperature of the first particle, $\theta_1(x^*)$, for a constant temperature plate.
Figure 13	Comparison of heat transfer for the discrete particles and a one-component continuum.
Figure 14	Dimensionless wall temperature distribution for a constant heat flux plate.
Figure 15	Average Nusselt number as a function of Péclét number for the discrete particle model.

Figure 16 Comparison of the discrete particle solution with a continuum with conductance K at the plate surface, for a constant temperature plate.

Figure 17 Comparison of the discrete particle solution with a continuum with conductance K at the plate surface, for a constant heat flux plate.

Figure 18 Typical particle arrangement in an actual flow, with increased voidage near the wall.

Figure 19 Schmidt plot results for the temperature distribution in a laminated medium, with $k_p \rho_p c_p / k_g \rho_g c_g$ equal to 4.

Figure 20 Schematic diagram of the flow apparatus.

Figure 21 Schematic diagram of the flat plate model.

Figure 22 Nusselt number versus Péclét number data for the .6" plate.

Figure 23 Nusselt number versus Péclét number data for the 1" plate.

Figure 24 Nusselt number versus Péclét number data for the mustard seed, using the .6" and 1" plate.

Figure 25 Modified Nusselt number versus modified Péclét number data for all materials tested, with both plate lengths.

Figure A-1 Central plate segment schematic indicating heat losses.

Figure B-1 Particle size histograms for glass traffic beads and glass impact beads.

Figure B-2 Particle size histogram for fine-grained sand.

Figure B-3 Particle size histogram for mustard seed.

Figure B-4 Schematic diagram of apparatus used for diffusivity measurements.

Figure B-5 Typical temperature-time plot for the diffusivity experiment.

Figure B-6 Section of the cylinder wall as modified for the specific heat measurement.

Figure B-7 Typical temperature-time plot for the specific heat experiment.

TABLE OF CONTENTS

		Page
	Acknowledgments	ii
	Abstract	iii
	List of Figures	iv
	Introduction	1
I.	Flow of Granular Materials	4
	A. Qualitative Observations	4
	B. Analytical Description	7
	1. Constitutive Equations	7
	2. Equations of Motion	10
	3. Radial Body Force Solution	11
II.	Heat Transfer from the Flat Plate	17
	A. General Remarks	17
	B. The Discrete Particle Model	19
	1. Comparison of the Discrete Particle Model with a One-Component Continuum	24
	2. The Flat Plate with Constant Heat Transfer Rate	26
	3. Other Comparisons	28
	4. Concluding Remarks on the Discrete Particle Model	30
	C. Experimental Investigations	33
	1. Dimensional Analysis	33
	2. Experimental Apparatus	38
	3. Measurement Techniques	42

Page

C. Experimental Investigations (continued)
4. Experimental Procedures 43
5. The Materials Investigated 44
6. Experimental Results 45

D. Discussion and Concluding Remarks 50

References 56

Appendix A 58

Appendix B 61

References (Appendices) 68

Tables and Figures 69

INTRODUCTION

The general problem to which the present study is directed concerns the convective heat transfer from surfaces immersed in a flowing granular material. The particular type of flow to be considered is that in which adjacent particles are in actual physical contact and the stresses in the material are transmitted primarily through these interparticle contacts. These contact-dominated flows are found to occur in certain industrial heat exchange equipment designed to heat, cool or dry granular materials [1,2][1]. It is to be noted that contact-dominated flows differ considerably from the more frequently investigated two-phase or "fluidized" granular flows where the interstitial fluid provides the major means of load transmission.

Section I of this thesis deals specifically with some of the unique features of contact-dominated particle flows. The main purpose of this section is to summarize the previous work that has been done regarding the flow of granular materials. After some discussion of the qualitative aspects of granular flow, a flow theory, proposed by other writers, is briefly described and the relevant equations which follow from this theory are developed. An exact solution, developed in the course of this research, to these equations is shown for the case of flow through a frictionless converging channel with a body force directed toward the channel vertex. This solution, which has

[1]Numbers in brackets indicate References listed at the end of the paper.

applications regarding the mass flow rate of granular materials through hoppers and bins, indicates features of the flow which agree with previously published experimental data.

A review of the literature on convective heat transfer to granular media revealed little fundamental information which would be of use to designers of granular flow heat exchangers. The data that are available include an experimental and theoretical study of the heat transfer to contact-dominated granular flows in long, smooth tubes by Brinn, et al [3] and experimental measurements of the heat transfer from cylindrical bodies immersed in a flow by Kurochkin [4]. Although both of these investigations consider the heat transfer from geometries having characteristic lengths much larger than the granular particle size, the two investigators arrive at different conclusions: Kurochkin found the particle diameter to be a significant variable governing the heat transfer from his cylinders, while Brinn, et al, demonstrated that their experimental results agreed with theoretical results based on the treatment of the granular material as a one-component continuum. Another experimental study, by Harakas and Beatty [5], considered the heat transfer from a flat plate immersed in a rotating granular bed. In this work, the fine-grained materials tested were found to behave like a one-component continuum except under vacuum conditions, when substantial deviations from the continuum prediction were observed. Thus, the previously published heat transfer data does indicate that under certain conditions the granular nature of the media may directly and substantially influence

the heat transfer.

Section II of the thesis deals specifically with granular flow convective heat transfer. The work to be discussed was planned to provide additional data on convective heat transfer, although particular emphasis has been placed on the effect of particle size, in view of the conflicting data in the literature. The objectives of the study are to determine the conditions for which the particulate nature of the media affects the heat transfer and to develop suitable correlations to account for this influence.

The specific geometry chosen for the investigation is the thin flat plate, oriented so the long axis of the plate is parallel to the flow field. This geometry has been selected since it represents one of the simplest and most basic convection problems and the results will be indicative of the general convective characteristics of granular media. In addition, the convective heat transfer from the plate for the observed flow field, a simple rectilinear flow parallel to the plate, can be analytically determined assuming the medium to be a one-component continuum. The experimental measurements may then be compared with this analytical solution to assess the effect of the "graininess" of the medium on the heat transfer.

I. FLOW OF GRANULAR MATERIALS

A. Qualitative Observations

As was mentioned in the Introduction, the type of particle flow under consideration here is that in which material stresses are transmitted chiefly through the interparticle contacts. The class of flow will now be further restricted to non-cohesive materials, that is, materials which cannot maintain tensile forces at the interparticle contact points. This class includes most materials consisting of hard, dry granules.

To obtain a flow dominated by interparticle contact forces with non-cohesive materials, the physical condition of flow must be such that the contact stresses are compressive, as otherwise the particles will separate. Typical examples of commonly encountered situations which lead to contact-dominated flows are the gravity flow of solids through hoppers and channels, and the flow around objects drawn through stationary granular beds.

To examine some qualitative aspects of contact-dominated flows, a vertical channel with transparent plexiglass walls was constructed. This channel, the specific construction details to be discussed in Section II, is provided with a constricted opening at its lower end, resulting in a contact-dominated gravity flow upstream of the opening. Various models can be placed in the channel and the flow around the models visually examined.

Figures 1(a) and 1(b) show, for example, the downward flow of a fine-grained, non-cohesive sand around a 1 in. diameter cylinder at two different velocities (approximately 2 and .2 inches per second for Figures 1(a) and 1(b), respectively). One feature of these flows is that a few diameters upstream or downstream of the cylinder, the flow in the channel is essentially rectilinear. Closer visual examination of the flow reveals that the particles adjacent to the smooth plexiglass wall slide along the wall at approximately the same speed as the bulk flow. Thus, there is no velocity boundary layer near smooth walls, as is the case with viscous fluid flows. This same observation was made, incidentally, by Brinn, et al [3] with regard to the flow of sand through smooth tubes.

A more striking feature of the flow around the cylinder is the cavity which appears immediately downstream of the cylinder. The size of this cavity evidently depends on the flow velocity, but even for very slow velocities, a small cavity remains. Apparently, the geometry of the cylinder is such that the filling of the void would require tensile stresses in the material beneath the cylinder under flow conditions, and such a state of stress cannot be maintained with the non-cohesive material used for the flow.

The upstream face of the cylinder also exhibits an unusual effect. The triangularly shaped region on top of the cylinder is stagnant, the size and shape of this zone being relatively insensitive to the flow velocity.

Not every geometry in a granular flow produces upstream stagnant zones or downstream cavities. The thin double wedge, shown in Figure 2, does not exhibit either effect at the flow velocity (approximately 2 inches per second) examined. However, at substantially higher velocities, the order of 4 inches per second, a cavity does begin to form at the side corners of the wedge.

Although no measurements were made here of material density variations in a granular flow, other authors [6, 7] have reported that the density variations in steady flow are small. The density appropriate for a steady granular flow corresponds to the "critical" void ratio, a concept used in soil mechanics referring to the void ratio obtained in a granular material after large, non-rigid deformation from a more or less densely packed initial state. This critical void ratio is largely independent of the mechanical stresses present [8], and thus the observation that the density is nearly constant in granular flow is not surprising. While it is assumed, for the present purposes, that granular materials flow at constant density, it is important to note that this assumption is generally not suitable for incipient flow problems, as demonstrated by the sequence of photographs on cylinder flow shown in Figure 3. Here, the fine-grained sand is placed in a compacted, dense state marked with alternate layers of colored sand. A complicated transition is seen to occur from the initial startup of flow until a steady state is obtained. Examination of the motion of the colored bands of material indicates that this transition is characterized by the expansion of the sand from its initial dense state to the final, critical density associated with steady flow.

B. Analytical Description

Mathematical models to describe the behavior of continuously flowing granular materials can be formulated beginning with a set of constitutive laws relating the material stresses to the deformations in a granular solid. One proposed set of constitutive laws, due to Jenike and Shield [9], will be briefly described in the following section. For additional details on this formulation[1], the reader is referred to the original paper [9].

1. Constitutive Equations

In Jenike and Shield's approach the flowing granular medium is modeled by an isotropic, incompressible, rigid-plastic continuum. The material is assumed to behave rigidly, unless subjected to a state of stress satisfying a yield condition. The particular yield condition used is the Mohr-Coulomb criterion, a criterion commonly used in soil mechanics [10]. In two-dimensional flow, for material elements subjected to a combination of positive compressive stresses[2] σ_{xx}, σ_{xy} and τ_{xy} referred to the x-y coordinate system, the Mohr-Coulomb yield condition is

$$\sqrt{\frac{(\sigma_{xx}-\sigma_{yy})^2}{4}+\tau_{xy}^2} = \frac{\sigma_{xx}+\sigma_{yy}}{2}\sin\delta . \qquad (1)$$

---

[1] The discussion here will be concerned with two-dimensional flows. A more general, and more complex, three-dimensional formulation is in [9].

[2] These stresses are "effective" stresses in the soil mechanics sense [11], i.e., the total mechanical stresses minus the interstitial fluid pore pressure.

This expression may be alternatively stated in terms of the principal stresses σ_1 and σ_2 as

$$\frac{\sigma_1-\sigma_2}{2} = \frac{(\sigma_1+\sigma_2)}{2} \sin\delta , \quad \sigma_1 \geq \sigma_2$$

where σ_1 and σ_2 are respectively the major and minor principal stresses in the x-y plane. The angle δ, a material property called the angle of internal friction, is a measure of the maximum shearing stress $\frac{\sigma_1-\sigma_2}{2}$ a material element can maintain at yield when subjected to a hydrostatic stress $\frac{\sigma_1+\sigma_2}{2}$. Equation (1) is often stated as an inequality, since states of stress leading to a maximum shearing stress less than that required by (1) are permitted, but only for rigid body motions of the material. However, in the <u>deforming</u> region of a granular flow only states of stress satisfying (1) may occur.

The second part of the constitutive formulation concerns the deformations which may occur when a material element is subjected to a state of stress satisfying the yield condition. The deformations are postulated to be such that:

(i) the material deforms at constant density;

(ii) the principal axes of the stress and strain rate tensors must coincide;

(iii) the rate of work done in deforming any material element is positive.

For two-dimensional flow, these postulates imply, respectively, that

$$\dot{\epsilon}_{xx} + \dot{\epsilon}_{yy} = 0 \qquad (2)$$

$$\frac{\sigma_{xx}-\sigma_{yy}}{\tau_{xy}} = \frac{\dot{\epsilon}_{xx}-\dot{\epsilon}_{yy}}{\dot{\epsilon}_{xy}} \tag{3}$$

$$\sigma_{xx}\dot{\epsilon}_{xx} + \sigma_{yy}\dot{\epsilon}_{yy} + \tau_{xy}\dot{\epsilon}_{xy} \geq 0 \tag{4}$$

where

$$\dot{\epsilon}_{xx} = \frac{\partial V_x}{\partial x} \; ; \; \dot{\epsilon}_{yy} = \frac{\partial V_y}{\partial y} \; ; \; \dot{\epsilon}_{xy} = \frac{1}{2}\left[\frac{\partial V_y}{\partial x} + \frac{\partial V_x}{\partial y}\right]$$

are the components of the strain rate tensor, shown here in terms of the Eulerian velocity components V_x and V_y.

Equations (1) through (4) represent the constitutive relationship proposed by Jenike and Shield for the two-dimensional, constant density flow of granular media. It is notable that the only material properly entering this model is the angle of internal friction δ. There are no fluid-like "rate" effects in that for given stress and strain rate fields, if all the strain rates are changed by some common factor, the stresses are unchanged. This characteristic of the model is consistent with the physical behavior of granular materials on testing machines.

While the constitutive laws just presented will be assumed for the purposes of this paper to be a reasonable reflection of the physical performance of actual granular materials in the continuum limit, it should be pointed out that the constitutive behavior of granular materials is a subject of continuing research. There have been, for example, alternative theories proposed by others [12, 13] which differ in detail with the Jenike-Shield model, particularly with regard to the kinematic

postulate (ii). These alternative theories have the disadvantage of relatively increased complexity without concrete experimental evidence to indicate that the added complexity actually results in a more realistic model and thus will not be considered further here.

2. Equations of Motion

The equations of motion may be written in terms of the effective stresses and the interstitial fluid pore pressure p as

$$\frac{\partial \sigma_{xx}}{\partial x} + \frac{\partial \tau_{xy}}{\partial y} + \frac{\partial p}{\partial x} + B_x = -\rho\left[V_x \frac{\partial V_x}{\partial x} + V_y \frac{\partial V_x}{\partial y}\right] \tag{5}$$

$$\frac{\partial \sigma_{yy}}{\partial y} + \frac{\partial \tau_{xy}}{\partial x} + \frac{\partial p}{\partial y} + B_y = -\rho\left[V_x \frac{\partial V_y}{\partial x} + V_y \frac{\partial V_y}{\partial y}\right] \tag{6}$$

where B_x and B_y are body forces in the negative x and y directions, respectively. In (5) and (6), the right-hand terms result from the inertia of the flow, and ρ is the bulk density of the granular material. The interstitial fluid pore pressure gradient appearing in these equations must be determined by examining the behavior of the interstitial fluid. It will be assumed that the interstitial fluid satisfies Darcy's law, that is

$$\kappa \vec{\nabla} p = (\vec{V}_f - \vec{V})$$

where κ is the permeability of the medium, $\vec{V}_f$ the superficial pore fluid velocity and $\vec{V}$ the bulk granular velocity. Since the interstitial fluid at the velocities encountered flows at constant density, it follows that

$$\vec{\nabla}^2 p = 0 \tag{7}$$

since the bulk material is also incompressible. In many applications, for example, the gravity flow through a channel with impermeable walls and upper and lower free surfaces exposed to atmospheric pressure, the solution to (7) is simply $p = 0$ in the channel and the interstitial fluid has no direct effect on the equations of motion.

The equations of motion together with the pore pressure equation (7), the constitutive postulates (1) - (4), and an appropriate set of boundary conditions provide a system to determine the three unknown effective stresses, the pore pressure, and the material velocity for the two-dimensional, non-rigid flow of granular materials. To demonstrate some of the consequences of this formulation, an exact solution, developed in the course of this study, will be presented.

3. The Radial Body Force Solution

The problem under consideration (see Figure 4) is the flow of a granular material through a converging, straight-sided channel with frictionless walls. The surfaces at $r = R$ and $r = r_o$ are stress-free and exposed to atmospheric pressure, and the material is subjected to a radially directed body force of magnitude ρg. This system should be representative of the gravity flow through a planar, frictionless funnel for small funnel vertex angles, θ_ω.

Referring now to the cylindrical coordinates r, θ, a solution of the following form is assumed:

$$\left.\begin{aligned} V_r &= V_r(r)\,; \quad V_r(r) \geq 0 \\ V_\theta &= 0 \end{aligned}\right\} \tag{8}$$

$$\left.\begin{aligned} \sigma_{rr} &= S(r)[1 - \sin\delta]; \quad S(r) \geq 0 \\ \sigma_{\theta\theta} &= S(r)[1 + \sin\delta] \\ \tau_{r\theta} &= 0 \\ p &= 0 \end{aligned}\right\} \qquad (8) \text{ cont.}$$

By direct substitution into the relevant equations expressed in cylindrical coordinates, it is seen that (8) satisfies the yield condition (1), the kinematic condition (3), and the requirement (4) that the plastic work be positive. The incompressibility condition (2) requires that

$$V_r(r) = \bar{V}\frac{r_0}{r}$$

where $\bar{V}$ is the radial velocity at the exit surface r_0.

The equation of motion in the θ direction, with a radially directed body force, is satisfied identically by (8), but the equation of motion in the r direction leads to

$$\frac{dS}{dr}(1-\sin\delta) + 2\frac{S}{r}\sin\delta + \rho g = \rho\left(r_0\frac{\bar{V}^2}{r^3}\right). \qquad (9)$$

The homogeneous solution to (9) is

$$S_H = Cr^{2\sin\delta/1-\sin\delta},$$

C being an arbitrary constant. The body force term ρg and inertia term $\rho(r_0\bar{V})^2/r^3$ lead to the particular solution

$$S_p = \frac{\rho g r}{3\sin\delta - 1} - \rho\frac{\bar{V}^2}{2}\left(\frac{r_0}{r}\right)^2$$

for $\delta \neq \sin^{-1}(1/3)$, or to

$$S_p = \frac{3}{2}\rho g r \log r - \rho \frac{\overline{V}^2}{2}\left(\frac{r_0}{r}\right)^2$$

for $\delta = \sin^{-1}(1/3)$. Considering for the moment only the case $\delta \neq \sin^{-1}(1/3)$, the complete solution to (9) is

$$S(r) = S_H + S_p = Cr^{2\sin\delta/1-\sin\delta} + \frac{\rho g r}{3\sin\delta - 1} - \rho \frac{\overline{V}^2}{2}\left(\frac{r_0}{r}\right)^2 .$$

The boundary condition $S = 0$ at $r = R$ determines the constant C, resulting in

$$S = \frac{\rho g r}{3\sin\delta - 1}\left[1 - \left(\frac{r}{R}\right)^{3\sin\delta - 1/1-\sin\delta}\right] - \rho \frac{\overline{V}^2}{2}\left(\frac{r_0}{r}\right)^2\left[1 - \left(\frac{r}{R}\right)^{2/1-\sin\delta}\right] .$$

The boundary condition on the lower free surface ($S = 0$ at $r = r_0$) can only be satisfied for a particular value of the exit velocity $\overline{V}$, namely

$$\frac{\overline{V}^2}{r_0 g} = \frac{2}{3\sin\delta - 1}\,\frac{\left[1-(r_0/R)^{3\sin\delta-1/1-\sin\delta}\right]}{\left[1-(r_0/R)^{2/1-\sin\delta}\right]} \qquad \delta \neq \sin^{-1}(1/3) .$$

Proceeding similarly for the case $\delta = \sin^{-1}(1/3)$, it follows that

$$\frac{\overline{V}^2}{r_0 g} = \frac{3\log(R/r_0)}{1-(r/R_0)^3} \quad , \quad \delta = \sin^{-1}(1/3) = 19.5^\circ .$$

In Figure 5, the group $\overline{V}^2/r_0 g$ is plotted versus R/r_0 to show the effect of the material head above the opening on the exit velocity. Of interest is the fact that for $\delta > \sin^{-1}(1/3)$, the exit velocity is independent of the material head for large R/r_0, the limiting value given by

$$\frac{\overline{V}^2}{r_0 g} = \frac{2}{3\sin\delta - 1} \qquad \delta > \sin^{-1}(1/3) .$$

This result is notable because it reflects the often observed experimental facts [14,15] that the exit velocity of granular solids through channels is proportional to the square root of the channel opening dimension and independent of the material head, provided the head is sufficiently high.

For $\delta \leq \sin^{-1}(1/3)$, the radial body force solution predicts that the exit velocity continuously increases with material head, a fluid-like phenomenon. The tendency for flow to be head independent or head dependent for angles of friction above or below $\sin^{-1}(1/3) = 19.5°$, respectively, has not been observed in practice, but this is not surprising since there are essentially no materials with an angle of internal friction below 19.5°.

Solutions can be obtained in an analogous manner for axially symmetric conical channels with a radial body force. In this solution, the circumferential stress in the channel is taken to be equal in magnitude to the major principal stress in the meridian plane[1], and the exit velocity for infinite material head is found to be

$$\frac{\overline{v}^2}{r_0 g} = \frac{2}{5 \sin \delta - 1} \qquad \delta > \sin^{-1}(1/5).$$

For $\delta \leq \sin^{-1}(1/5)$, the flow velocity does not become independent of the head, analogous to the case $\delta \leq \sin^{-1}(1/3)$ for plane channels.

In the course of the present investigation, a few experimental measurements were made of the flow rate through plane and conical

---

[1] This is a consequence of the three-dimensional constitutive law in [9].

channels of various vertex angles θ_w. Two non-cohesive materials, a fine-grained sand and small glass beads (.01 inch diameter), with different angles of internal friction were used in the tests, in conjunction with relatively rough and smooth channel walls. The results are shown in Figures 6 through 9, in terms of the dimensionless exit velocity $\overline{V}/\sqrt{Dg}$ as a function of channel opening angle θ_w. Here, D in the group $\overline{V}/\sqrt{Dg}$ refers to the channel exit width for plane channels, or the opening diameter for conical channels. The data are in fair agreement with the empirical correlation of Johanson [16] shown as a dotted line in the figures. The radial body force solution expressed in terms of the group $\overline{V}/\sqrt{Dg}$ predicts a qualitatively correct flow rate dependence on θ_w. However, the magnitude of the predicted flow rate is considerably higher than that observed experimentally. This divergence is believed to be due to the Coulomb-frictional forces acting along the walls of the experimental channels, these forces having a tendency to retard the flow.

Other authors [17, 18] have provided numerical solutions to the channel flow problem, including Coulomb friction along the walls, with the assumption of "creeping" flow, that is, negligible flow inertia. While this approximation may lead to an accurate stress distribution far from the orifice where material inertia is, in fact, negligible, the approximation is not suitable for predicting the mass flow rate since the resulting velocity fields are determined only to within an arbitrary, positive multiplicative factor. Although the radial body force solution shows clearly that the anomaly in the velocity field may be rectified by

retaining the inertia terms in the equations of motion, it appears that mathematical solutions to the complete equations have not been found for channel flow with Coulomb friction at the walls. This particular problem, as well as the search for other solutions to the flow equations remains a subject for future research on the flow of granular materials.

In Section II to follow, the emphasis is shifted from the flow of granular materials to convective heat transfer in granular flow. The particular problem to be considered, the convective heat transfer from a smooth flat plate, involves a rigid-body flow field and consequently the details of the flow analysis presented above will not be used to determine the velocity field associated with this problem. Certain facts discussed in Section I on granular flow are, however, important for the subsequent work on heat transfer. Specifically, the observation that the flow field in a channel with smooth parallel walls is rectilinear, and the fact that granular materials flow at essentially constant density corresponding to the critical void ratio of the material, will be referred to frequently.

II. HEAT TRANSFER FROM THE FLAT PLATE

A. General Remarks

In considering the general problem of convective heat transfer from bodies immersed in a flowing granular medium, an approach analogous to that used in fluid mechanics seems appropriate. This approach would involve treating the medium as a continuum, applying the equations of flow to determine the velocity distribution about the body, and then using this velocity field in the convective energy equation to obtain the temperature distribution in the medium and the heat flux from the body. This is, of course, quite simply stated but in practice a difficult process as the appropriate equations, particularly those governing the flow, are complex and analytical solutions are not readily obtained. There is, however, aside from these very real practical difficulties, a fundamental question which should be answered before the fluid mechanics type of approach may be used: under what conditions can the medium be considered to behave as a continuum? Clearly, if a continuum approach predicts substantial changes in velocity or temperature over distances the order of the particle characteristic length, the results are not likely to reflect what actually occurs in a physical system, at least not in the neighborhood of the large gradients. In convective heat transfer problems experience with Newtonian fluids indicates that near the heated surface of a body immersed in a flow, large temperature changes occur over

small distances, within the thermal boundary layer. In a granular flow, therefore, the possibility exists that even if the particles are "small" with respect to the characteristic length of the heated surface, the thermal boundary thickness could be the same order as the particle size, resulting in substantial deviation from heat transfer rates predicted by a continuum theory.

In order to determine under what conditions, if any, these non-continuum effects might be observed, the flat plate with its long axis parallel to the granular flow is considered for specific analytical and experimental studies. This simple geometry was chosen chiefly because the flow field consists of a uniform velocity parallel to the plate (provided the plate is smooth), and thus the issue of non-continuum effects in heat transfer is not confused by complexities in the flow field.

In what follows, an idealized granular material, referred to as the "discrete particle model", is studied for the purpose of gaining insight regarding the magnitude and nature of any non-continuum effects associated with the heat transfer from the flat plate. Finally, experimental measurements of flat plate heat transfer rates are presented and discussed.

B. The Discrete Particle Model

This model is an idealized granular material with the following properties:

(i) The particles have infinite thermal conductivity, and are spherical with uniform diameter d;

(ii) The particles flow past the heated plate in an orderly array, as shown in Figure 10, and extend indefinitely in the y direction. The temperature of the particles far from the heated plate is T_∞;

(iii) Heat is transferred only between adjacent particles, the heat flow from particle to particle given by $q = \overline{K}\Delta T_p$, where $\overline{K}$ is the particle to particle conductance and ΔT_p the temperature difference between particles;

(iv) Particle to particle heat transfer in the x direction is negligible compared with particle to particle heat transfer in the y direction. This simplification is analogous to the boundary layer approximation used in continuum heat transfer.

Suppose that this idealized medium is subjected to a steady, one-dimensional heat flow between two parallel plates, separated by a distance ℓ much larger than the particle diameter. The thermal conductivity k of the composite is defined by

$$k = q'' \frac{\ell}{\Delta T}$$

where q'' is the heat flow rate per unit area, and ΔT is the temperature difference between the parallel plates. This bulk conductivity k can be

related to the particle to particle conductance $\overline{K}$ as follows. Noting that for n particles between the plates, $\ell = nd$ and $\Delta T = n\Delta T_p$, and since there are $1/d^2$ particles per unit area of the plate, the heat flow per particle is $q = q'' d^2$. Using these relationships, and property (iii) of this idealized material to eliminate q'', ℓ and ΔT from the definition of k yields

$$k = \frac{\overline{K}}{d}.$$

Similarly, the density ρ and specific heat c of the composite are given by (neglecting the mass and heat capacity of the interstitial voids)

$$\rho = \frac{M}{d^3} \quad , \quad c = c_p \, ,$$

where M and c_p are the mass and specific heat of a typical particle.

The equations governing the heat transfer to the particles from the plate will now be developed. In Figure 11 a particular row of particles moving with uniform velocity U in the x direction is examined. Denoting the temperature of the j^{th} particle in Figure 11 by T_j, a heat balance for the j^{th} particle at time t yields (neglecting conduction in the x direction)

$$\overline{K}\left[T_{j-1} + T_{j+1} - 2T_j\right] = Mc \frac{dT_j}{dt}. \qquad j = 2,3,\ldots$$

Since the particles move at a uniform constant velocity U, the x coordinate of the particle centers, $x = Ut$, is used as a time scale. Then, the heat balance for the j^{th} particle becomes

$$\overline{K}\left[T_{j-1} + T_{j+1} - 2T_j\right] = McU \frac{dT_j}{dx}. \qquad j = 2,3,\ldots \tag{10}$$

The case in which the plate is maintained at constant temperature $T_w \neq T_\infty$ will be considered first. The temperature of the particle adjacent to the plate must satisfy

$$\overline{K}[T_w + T_2 - 2T_1] = McU\frac{dT_1}{dx} \qquad x \geq 0 \tag{11}$$

where it has been assumed that the conductance between the wall and adjacent particles is $\overline{K}$.

Since heat conduction does not occur in the x direction, the temperature upstream of the plate will be T_∞ uniformly, i.e.,

$$T_j = T_\infty \qquad j = 1,2,\ldots \qquad x \leq 0 \tag{12}$$

Equations (10) - (12) are conveniently expressed in terms of the dimensionless temperature $\theta_j = (T_j - T_w)/(T_\infty - T_w)$, and the dimensionless length $x^* = \frac{x\overline{K}}{McU}$. Substituting these new variables into (10) - (12) leads to

$$\theta_{j-1} + \theta_{j+1} - 2\theta_j = \frac{d\theta_j}{dx^*} \qquad j = 2,3,\ldots \tag{13}$$

$$\theta_2 - 2\theta_1 = \frac{d\theta_1}{dx^*} \qquad x^* \geq 0 \tag{14}$$

and

$$\theta_j = 1 \qquad j = 1,2,\ldots ; \; x^* \leq 0 \tag{15}$$

The solution $\theta_j(x^*)$ of the system of equations (13), (14) and the boundary condition (15) will now be deduced. To eliminate the derivative in the system of differential equations (13), let $\theta_j = C_j e^{\lambda x^*}$, where λ is, for the moment, an arbitrary constant. Substituting this expression for the θ_j into (13), the following equations result:

$$(\lambda+2)C_j = C_{j-1} + C_{j+1} \qquad j=2,3, \ldots . \tag{16}$$

A solution to (16), as can be verified by direct substitution, is given by

$$C_j = Ce^{ji\nu} \tag{17}$$

where i is the unit imaginary number, C is an arbitrary constant, and ν is related to λ through

$$\lambda+2 = e^{i\nu}+e^{-i\nu} = 2\cos\nu .$$

Since (16) does not involve any complex constants both the real and imaginary parts of (17) should satisfy (16), hence the C_j can alternatively be written using sine and cosine functions,

$$C_j = A\sin j\nu + B\cos j\nu .$$

However, the substitution of this expression into the heat balance for the first particle (14) shows that B must vanish.

Thus, the form

$$\theta_j^*(x^*) = A\sin j\nu e^{(2\cos\nu-2)x^*} \qquad x^* \geq 0$$

is a solution to the system of equations (13) and (14) for any choice of A or ν. This solution, however, does not satisfy the condition that $\theta_j = 1$ at $x^* = 0$. But since the equations involved are linear, the infinite sum of integrals

$$\theta_j(x^*) = \sum_{m=1}^{\infty} \int_0^{\pi} A_m(\nu)\sin j\nu e^{(2\cos\nu-2)x^*}\, d\nu$$

is also a solution, assuming this series converges. The choice $A_m(\nu) = \frac{2}{\pi}\sin m\nu$ yields $\theta_j(0) = 1$ for all j, therefore, the solution to the equations and boundary conditions presented is

$$\theta_j(x^*) = \frac{2}{\pi} \sum_{m=1}^{\infty} \int_0^{\pi} \sin m\nu \sin j\nu e^{(2\cos\nu - 2)x^*} \, d\nu \qquad (18)$$

for $x^* \geq 0$. This equation may be expressed in terms of tabulated functions by using the identity

$$\sin m\nu \sin j\nu = \frac{1}{2} \{\cos (m-j)\nu - \cos (m+j)\nu\}$$

and noting that (see Reference [19]),

$$\int_0^{\pi} e^{2x^*\cos\nu} \cos n\nu \, d\nu = \frac{\pi}{2} I_n(2x^*)$$

where I_n is the modified Bessel function of the first kind. Upon application of these results, (18) becomes

$$\theta_j(x^*) = e^{-2x^*} \left[I_0(2x^*) - I_j(2x^*) + 2 \sum_{m=1}^{j} I_m(2x^*) \right] .$$

Of particular interest is $\theta_1(x^*)$, shown in Figure 12, since the heat flow at the wall due to an individual particle at position x^* is given by

$$q(x^*) = \overline{K}(T_w - T_\infty)\theta_1(x^*) .$$

The average heat $\overline{q}$ removed per unit time by a particle traversing a plate of length L is

$$\overline{q} = \frac{1}{L} \int_0^L q(x^*) \, dx.$$

Since there are $1/d^2$ particles per unit area, the average heat flux from the plate $\overline{q}''$ is $\overline{q}/d^2$. Using the usual definition for the average film coefficient, $\overline{h} = \overline{q}''/T_w - T_\infty$, the Nusselt number $\overline{Nu}_L = \overline{h}L/k$ for the

discrete particle flow is

$$\overline{Nu}_L = \frac{\bar{K}}{d^2 k} \frac{L}{L^*} F(L^*)$$

where $L^* = L\bar{K}/McU$ and

$$F(L^*) = \int_0^{L^*} \theta_1(x^*)\, dx^*.$$

The Nusselt number may be expressed in terms of the bulk properties of the medium, in particular the conductivity $k = \bar{K}/d$ and diffusivity $\alpha = k/\rho c = \bar{K}d^2/Mc$

$$\overline{Nu}_L = \frac{d}{L} Pe_L F\left\{\left(\frac{L}{d}\right)^2 \frac{1}{Pe_L}\right\}$$

In this expression Pe_L is the Péclét number, defined as $Pe_L = UL/\alpha$.

1. Comparison of the Discrete Particle Model with a One-Component Continuum

For purposes of comparison, the heat transfer from the flat plate associated with the uniform flow of a one-component continuum with properties k and α can be determined within the boundary layer approximation of negligible conduction in the x direction. For this continuum flow, the energy equation is

$$\frac{\partial^2 T}{\partial y^2} = \frac{U}{\alpha} \frac{\partial T}{\partial x} \tag{19}$$

and with the constant temperature flat plate, the boundary conditions are

$$\left.\begin{aligned} T(0,x) &= T_\omega \quad x \geq 0 \end{aligned}\right\} \tag{20}$$

$$\left.\begin{aligned} T(0,x) &= T_\infty \quad x<0 \\ T(\infty,x) &= T_\infty \,. \end{aligned}\right\} \qquad (20)\ \text{cont.}$$

Noting that (19) is identical in form to the well-known heat diffusion equation, the solution for the local film coefficient is given by

$$h(x) = \frac{q''(x)}{T_w - T_\infty} = \frac{k}{\sqrt{\pi}} \frac{1}{\sqrt{\alpha x/U}}$$

Integrating this expression over a plate of length L yields the average Nusselt number,

$$\overline{Nu}_L = \frac{2}{\sqrt{\pi}} \sqrt{Pe_L} \,. \qquad (21)$$

To compare the heat transfer result of the discrete particle model to the continuum, the ratio of the Nusselt number obtained for these different materials is illustrative.

$$R = \frac{\overline{Nu}_L(\text{discrete particles})}{\overline{Nu}_L(\text{continuum})} = \frac{\sqrt{\pi}}{2} \frac{F(\eta)}{\sqrt{\eta}}$$

where

$$\eta = \left(\frac{L}{d}\right)^2 \frac{1}{Pe_L}$$

This ratio is plotted in Figure 13, and this curve indicates that for $\eta < 10$, the discrete particle model deviates considerably from the continuum prediction. Of interest is the fact that this deviation is a function of the single dimensionless group η. This variable can be given a physical interpretation by means of the continuum solution,

which shows that the dimensionless thermal boundary layer thickness δ/L is proportional to $1/\sqrt{Pe_L}$. Thus,

$$\frac{\delta}{d} \alpha \frac{L}{d}\Big/\sqrt{Pe_L} = \sqrt{\eta}$$

represents the ratio of the thermal boundary layer thickness to the particle diameter.

2. The Flat Plate with Constant Heat Transfer Rate

Another problem of interest is when a constant heat flux, rather than temperature, is specified along the plate.

With the continuous material, the heat transfer equation (19) still applies, but the first boundary condition in (20) is replaced by

$$-k\frac{\partial T}{\partial y}(0,x) = q'' = \text{const.} \qquad x \geq 0$$

for the constant heat flux problem. The solution to (19) with this boundary condition (see, for example, [20]) expressed in terms of the average Nusselt number results in

$$\overline{Nu}_L = \frac{3}{4}\sqrt{\pi}\sqrt{Pe_L}.$$

For the discrete particle model, an indirect method has been used to obtain the constant heat flux solution. The basic steps of this solution will be briefly outlined. Since the system of equations describing the medium is linear, the principle of superposition applies. Therefore, the solution to the problem of a specified wall temperature $T^*_w(x)$ can be expressed, by application of Duhamel's theorem, in terms of an integral involving the solution for constant temperature wall

conditions and the distribution $T^*_w(x)$. Specifically, for the temperature $T^*_1(x)$ under conditions of a variable wall temperature $T^*_w(x)$, the solution is

$$T^*_1(x) = T_\infty + \int_0^x \frac{\partial}{\partial x}\left\{\theta_1(x-\xi)\right\}\left(T^*_w(\xi)-T_\infty\right)d\xi$$

where $\theta_1(x)$ is the solution shown previously for the constant temperature wall. The condition that the heat flux along the wall is constant may be stated as

$$T^*_w(x) - T^*_1(x) = \frac{q}{\overline{K}} = \text{const.} \qquad x \geq 0$$

Substituting the integral form for $T^*_1(x)$ in the constant heat flux condition results in an integral equation for the wall temperature $T^*_w(x)$. This equation may be solved using simple numerical iteration, to yield the wall temperature distribution $(T^*_w-T_\infty)/(q/\overline{K})$, shown in Figure 14 as a function of x^*. The average film coefficient $\overline{h}$ is defined by

$$\overline{h} = \frac{q''}{\overline{T}_w - T_\infty}$$

where

$$\overline{T}_w = \frac{1}{L}\int_0^L T^*_w(x)\,dx$$

is the average temperature of the wall. This film coefficient in terms of the Nusselt number $\overline{h}L/k$, is plotted in Figure 15 as a function of the Péclét number and the ratio L/d. The constant heat flux results differ only slightly in magnitude from the constant temperature plate

solution, which is also shown in Figure 15. In fact, in the limit as $\left(\frac{L}{d}\right)^2 \frac{1}{Pe_L}$ approaches zero, the two solutions are identical.

3. Other Comparisons

It is of interest to compare the heat flux calculated using the discrete particle model, which has thermal resistances between each particle, with a continuum having a single thermal resistance at the wall. Such a comparison should give some insight regarding the influence of the granular structure which is not adjacent to the wall on the overall heat transfer from the wall.

The temperature field associated with a continuum that has a thermal conductance K at the plate surface[1] must satisfy the convective heat transfer equation (19), with the first boundary condition in (20) replaced by

$$-k\frac{\partial T}{\partial y}(0,x) = K[T_w - T(0,x)] \quad x \geq 0$$

where T_w is the constant temperature of the plate. The solution to (19) with this boundary condition is found in [21] and yields the local film coefficient

$$\frac{h(x)}{k} = \frac{K}{k} e^{\beta_x^2} \operatorname{erfc}[\beta_x].$$

In this expression, $\beta_x = \frac{Kx}{k}\sqrt{\frac{1}{Pe_x}}$ and $\operatorname{erfc}[\beta_x]$ is the complimentary error function. Averaging this the local film coefficient over the plate gives

[1] K is the conductance per unit area of the plate, related to the particle to particle conductance through $K = \overline{K}/d^2 = k/d$.

$$\overline{Nu}_L = \frac{\bar{h}L}{K} = \frac{KL}{k}\left\{\frac{1}{\beta^2}\left(e^{\beta^2}\,\mathrm{erfc}\,(\beta) - 1 + \frac{2}{\sqrt{\pi}}\beta\right)\right\}$$

$$= \frac{KL}{k} f(\beta)$$

where

$$\beta = \frac{KL}{k}\sqrt{\frac{1}{Pe_L}}$$

To compare this result with the discrete particle solution, the latter must be expressed in terms of the same variables. Recall that for the discrete particle model with a constant temperature plate,

$$\overline{Nu}_L = \frac{d}{L} Pe_L F(\eta)$$

$$\eta = \left(\frac{L}{d}\right)^2 \frac{1}{Pe_L}$$

but,

$$\frac{L}{d} = \frac{KL}{Kd} = \frac{KL}{k},$$

hence $\eta = \beta^2$. Thus,

$$\overline{Nu}_L = \frac{KL}{k}\,\frac{F(\beta^2)}{\beta^2} = \frac{KL}{k} F^*(\beta)$$

for the discrete particles. In Figure 16 the function $F^*(\beta)$ associated with the discrete particle analysis is shown, as is the function $f(\beta)$ for the continuum with a single resistance at the wall. Also shown is the numerically approximate form $1/(1+\sqrt{\pi}/2\,\beta)$ for $f(\beta)$. For large β, both $f(\beta)$ and $F^*(\beta)$ converge to the asymptote $2/(\sqrt{\pi}\beta)$, this asymptote corresponding to the continuum solution, $\overline{Nu}_L = \frac{2}{\sqrt{\pi}}\sqrt{Pe_L}$. For smaller β, the continuum with resistance at the wall behaves like the discrete

particle model. It would seem, therefore, that as a first approximation for the Nusselt number in a discrete particle flow, only the first resistance between the wall and the particles need be considered.

Figure 17 compares the discrete particle model and a continuum with a resistance at the plate surface for a constant heat flux plate. These curves differ only slightly from the analogous set of Figure 16 for the constant temperature boundary condition. There is, however, an additional discrete particle solution shown for the constant heat flux plate which applies when the conductance between the first row of particles and the wall is K and the interior particle to particle conductance is K′. The dimensionless wall temperature distribution $(T^*_w - T_\infty)/(q''/K')$ for this case is calculated simply by adding the constant $(K'/K) - 1$ to the dimensionless temperature distribution obtained when all the conductances are equal to K′. The resultant Nusselt number for the modified wall temperature distribution is represented in Figure 17 for the case $(K'/K) = 2$. Note that this solution, which has a thermal resistance at the plate twice the size as the interior resistances, is closer to the prediction for a continuum with a single resistance of magnitude 1/K at the plate surface.

4. Concluding Remarks on the Discrete Particle Model

In closing the discussion on the discrete particle model, it is appropriate to review the major qualitative aspects of the heat transfer from a flat plate using this idealized non-continuous solid as the convecting medium. First, the average film coefficient for the discrete

particle flow can be substantially lower than for the flow of a continuous medium with the same bulk properties. The condition for this difference to occur is that the dimensionless group $(L/d)^2\ 1/Pe_L$, which is a measure of the ratio of the thermal boundary layer thickness to the particle diameter, be less than 10. Secondly, the average film coefficients for the constant temperature and constant heat flux plates are notable for their quantitative similarity. Finally, the Nusselt number for the composite medium is, to a first approximation, represented by that for a continuum with a single thermal resistance at the heated wall, an approximation which improves if the wall to particle thermal resistance is larger than the particle to particle resistances.

With regard to the flow and heat transfer using actual granular materials made up of spherical particles, there are some notable differences in the physical system and the idealized discrete particle system. For example, the array of particles is not regular, but rather like that shown in Figure 18. The fact that the particles adjacent to the wall are not as densely packed as those farther from the wall [22] could be particularly significant since the degree of packing near the wall will affect the wall to particle conductance. Also, the particles in a physical system have finite thermal conductivity and thus are capable of supporting temperature gradients. While it is not expected that deviations such as these from the discrete particle model will influence the qualitative nature of the non-continuum effects, it is expected that the numerical values of the predicted heat transfer coefficients will differ somewhat from any experimental results.

However, in planning the experiments, which are described in the next section, the discrete particle analysis was used as a guide, both for the design of the apparatus and for the presentation of data.

C. Experimental Investigations

1. Dimensional Analysis

Before discussing the details of the experimental apparatus and the data obtained, the principal dimensionless parameters governing the problem will be determined. In assessing what variables are significant, the discussion is restricted to granular media consisting of relatively hard, dense particles in a low density interstitial fluid, such as air. The development that follows is carried out for the specific case of spherical particles, all with the same diameter d. It is assumed that the geometry of the granular mass is completely specified, in the statistical sense, by the diameter d and void ratio ϵ of the composite. For more complicated materials, such as media with a wide distribution of spherical particle sizes, or with non-spherical particles, additional statistical quantities will generally be necessary to fully characterize the geometry of the medium.

To determine the variables needed to describe the thermal behavior of a granular medium, it is necessary to examine the basic mechanisms involved as heat is transferred from particle to particle. There are, evidently, three of these mechanisms:

(1) conduction through the interstitial gas;

(2) conduction through the physical interparticle contacts;

(3) thermal radiation across the voids.

A fourth possible heat transfer mechanism is convection due to the movement of the interstitial fluid with respect to the particles.

However, as was discussed in the preceding section on granular flow, most flow conditions result in the interstitial fluid moving with the particles, the pore pressure being everywhere a constant. Since the flow apparatus used in the experimental work to be described has all free surfaces exposed to atmospheric pressure, the pore pressure will be constant throughout the flow field, and thus interstitial fluid convective effects will not be considered in the following development.

Some insight into the relative contribution toward the total heat transfer by each of these mechanisms can be gained by studying measurements of the bulk conductivity of granular materials with a stagnant interstitial fluid. For example, data by Yagi and Kunii [24] and Schotte [25] show that for granular materials consisting of small particles (less than .12 inches diameter), the thermal conductivity is independent of the mean material temperature provided this temperature is below 800°R. This result suggests that at moderate temperatures, thermal radiation does not contribute significantly to the total particle to particle heat transfer. The condition ensuring that radiation be negligible in comparison to conduction can be estimated by noting that the ratio of radiative to conductive transfer between particles of diameter d with an interstitial gas of conductivity k_g is in rough proportion to $\sigma T^3 d/k_g$, where σ is the Stefan-Boltzman constant and T the average absolute temperature of the particles[1]. From Yagi and Kunii's data, the indication is that for values of this

[1] This relationship may be derived by considering the combined conduction and radiation between two "black" infinite parallel plates, separated by a distance d.

dimensionless group less than about .5, thermal radiation is relatively negligible, as reflected by the temperature insensitivity of the thermal conductivity data. For the present series of experiments, the ratio $\sigma T^3 d/k_g$ is generally less than .5, thus thermal radiation is not expected to be significant.

Other conductivity data by several authors are summarized in [25] for granular media with a wide range of particle conductivities. These data indicate that the bulk conductivity of granular materials below 800°R drops by a factor of 10 to 100 in a vacuum, compared to the conductivity with atmospheric air in the interstitial voids. This is another indication that the radiative contribution to the heat transfer is small when atmospheric air is the interstitial fluid, but more importantly, these data suggest that the heat transfer through the interparticle contacts is but small fraction of the heat conduction through the voids.

It is, on the basis of these data, taken as a reasonable approximation, which encompasses the majority of granular materials, that the interparticle heat transfer is solely by conduction through the interstitial medium. This approximation, of course, will not be reasonable for every granular material in every application. For example, if the interstitial medium has a conductivity substantially lower than air at atmospheric pressure, the relative balance of the three transfer mechanisms may then favor radiation across the voids and conduction through thephysical contacts. Or, if the material is subjected to high mechanical pressures, compared to the elastic constants of the particles, the particle to particle contact area could

increase enough to make conduction through the contacts of major importance. Physical conditions such as these, however, are relatively unusual and they will not be considered further.

Taking into account the preceding assumptions, then, it follows that for spherical particles of diameter d flowing at a void ratio ε over a plate of length L, the average film coefficient may be expressed in the form

$$\bar{h} = f(\rho_g c_g, \rho_p c_p, k_g, k_p, \varepsilon, d, L, U)$$

where the subscripts p and g denote properties of the particles and interstitial fluid, respectively. Implicit in this expression is the approximation discussed previously of negligible heat transfer by radiation or by conduction through the interparticle contacts.

Forming the appropriate dimensionless groups, the film coefficient may be expressed as

$$\frac{\bar{h}L}{k_p} = f_1\left[\frac{k_g}{k_p}, \frac{\rho_g c_g}{\rho_p c_p}, \frac{L}{d}, \frac{UL}{\frac{k_p}{\rho_p c_p}}, \varepsilon\right]$$

A more convenient form from an experimental point of view follows from the use of the bulk properties k and ρc of the composite. Then

$$\overline{Nu}_L = \frac{\bar{h}L}{k} = f_2\left[\frac{k_g}{k}, \frac{\rho_g c_g}{\rho_p c_p}, \frac{L}{d}, \frac{UL}{\alpha}, \varepsilon\right]$$

where $\alpha = k/\rho c$ is the bulk diffusivity of the medium.

A final simplification to be made utilizes the fact that the heat capacity per unit volume of the interstitial gas $\rho_g c_g$ is generally orders of magnitude less than the particle heat capacity, $\rho_p c_p$. To examine

the simplifying consequences of the small size of $\rho_g c_g/\rho_p c_p$, a laminated medium flowing at uniform velocity U past a flat plate is considered. This medium consists of alternate layers, each with thickness ℓ, of low density and high density materials, designated by the subscripts g and p, respectively. The temperature distribution in this medium, at various positions x from the leading edge of a plate at temperature T_w, is shown in Figure 19 as a function of

$$\left(\frac{x}{\ell}\right)^2 \frac{\alpha_g}{Ux},$$

where $\alpha_g = k_g/\rho_g c_g$. This distribution was determined approximately by using the Schmidt plotting technique [26] for the case when the ratio $k_p\rho_p c_p/k_g\rho_g c_g$ is 4, although essentially similar results are obtained for larger values of $k_p\rho_p c_p/k_g\rho_g c_g$. Note that for

$$\frac{x}{\ell^2}\frac{\alpha_g}{U} > .5,$$

the low density medium behaves quasi-statically, like a simple thermal resistance with negligible heat capacity. In the immediate vicinity of the leading edge of the plate, however, where

$$\frac{x}{\ell^2}\frac{\alpha_g}{U} << .5,$$

the low density material cannot be considered to have negligible heat capacity. For typical granular materials, the ratio $k_p\rho_p c_p/k_g\rho_g c_g$ is much larger than unity and it will be assumed that the interstitial gas surrounded by the high-density particles behaves quasi-statically, i.e., as if the gas has negligible heat capacity. This

assumption should be reasonable, for a plate of length L, if the ratio

$$\frac{x}{\ell^2}\,\frac{\alpha_g}{U}$$

becomes greater than .5 for values of x which are a small fraction of the plate length L. Here, ℓ is the effective "thickness" of the interstitial gas between the particles and the plate, which is the order of the particle diameter. Whether this condition is satisfied in the experimental tests conducted will be discussed later on in conjunction with the interpretation of the experimental results obtained.

With the assumption, then, of negligible heat capacity in the interstitial medium, the expression for the Nusselt number may be further simplified to the form

$$\overline{Nu}_L = F\left(\frac{k_g}{k}, \frac{L}{d}, \frac{UL}{\alpha}, \epsilon\right). \qquad (22)$$

In the experiments to be described subsequently, the parameters in (22) will be varied and the effect of these variations on the Nusselt number examined.

2. Experimental Apparatus

The flow apparatus, shown schematically in Figure 20, consists of three basic parts, from top to bottom: the supply hopper; the plexiglass test section; and the regulating valve.

The regulating valve is basically an adjustable clamp acting on a rubber membrane. This clamp provides a continuous adjustment

of the mass flow rate through the valve and is the means by which the velocity in the channel is controlled.

The test section is constructed of plexiglass to facilitate visual observation of the flow. Removable front and rear sections are provided for the mounting of models in the flow field. The flow area of the test section can be changed by adding area-reducing inserts, shown by the dotted lines in Figure 20. These inserts permit higher velocities to be maintained in the test section while keeping the mass flow rate within reasonable limits.

The supply hopper has considerably larger volume than the test section and enables flow to persist in the channel for several minutes. In the heat transfer experiments, continuous flow is required for an extended period, necessitating periodic refilling of the supply hopper through its open top.

The system as described is capable of maintaining a continuous velocity in the channel between approximately .2 and 2 inches per second, the exact limits depending on the particular material used in the flow. The lower limit on the velocity results from the inability of the flow valve to pass a steady flow without clogging at very low flow rates, and the upper limit from the difficulty in maintaining the level in the supply hopper at very high flow rates. The obtainable range, however, was entirely sufficient for the present program.

The flat plate used for the heat transfer experiment is shown in Figure 21. A pair of heated copper plates are imbedded on opposite

sides of the thin plexiglass holder which is placed in the flow channel with its long axis coincident with the channel centerline. The resulting symmetric flow will expose each plate to a similar flow field. This symmetry ensures that there will be no heat transfer across the model from one set of plates to the other. The central portion of the holder is hollowed out and the heated plates are separated by an air gap to leave room for the connecting wiring and the thin resistance heaters bonded to the interior surfaces of the copper plates. This air gap is filled with rock wool insulation to eliminate free convection in the gap. To reduce thermal conduction from the leading and trailing edges of the plate to the holder, a 1/16 inch air gap is provided at these edges, this gap being covered with cellophane tape to keep it from filling with granular material.

Referring to the front view of the plate (Figure 21), each plate is split into three segments separated by thin air gaps. The actual heat transfer measurements are made only on the central segment of the plate, which is provided with its own heating element. The outer plate segments act as guards, the individually adjustable heaters on the segments being regulated to equalize the temperatures of the central and outer plate segments. With the outer segments adjusted in this manner, no heat will be lost from the central segment in the transverse direction. It may then be assumed that all the heat supplied to the central heater is actually transmitted to the granular flow. Another reason for segmenting the plate is to isolate its central portion from the

edges of the flow field, so that the heat transfer from the central segment will be truly two-dimensional.

The resistance heating elements are fabricated with Nichrome wire and are electrically insulated from the copper plates. Each heater has a resistance of approximately 3 ohms and is connected in series with a 0-1 ohm variable bias resistor. The heater and bias resistor combinations are connected in parallel to an adjustable power supply which is operated in the neighborhood of 3 volts. By adjusting the appropriate bias resistor, the voltage across each heater may be regulated independently over a range adequate to permit temperature equalization of all the plate segments.

The plate length of 1 inch was selected, using the discrete particle analysis as a guide, so that measurable non-continuum effects would be encountered for the materials under investigation. A provision is made, however, to replace the 1 inch plate by a similar set with .6 inch length in the same holder, for the purpose of permitting the independent variation of the group L/D in (22).

Heat losses from the central plates are a source of error which must be carefully controlled, in view of the low heat transfer coefficients encountered with the typically poor-conducting granular materials under investigation. The major losses are due to heat conduction from the central segment to the plate holder, and to those outer segments which are not at exactly the same temperature as the central segment. Estimates of these losses, the calculations given in Appendix A,

indicate that for typical operating conditions these losses constitute 6% or less of the heat supplied to the central segment.

The distance from the surface of the plates to the walls of the flow channel, both with and without the area-reducing inserts installed, is many times the thermal boundary layer thickness estimated using a continuum theory. The channel wall is therefore expected to be effectively an infinite distance from the plate surface. This contention is checked experimentally by comparing heat transfer data obtained using the channel with and without the area-reducing inserts installed.

3. Measurement Techniques

Each plate temperature is measured with a chromel-alumel .005 inch diameter wire thermocouple, mounted by imbedding the chromel branch near the leading edge of the plate and the alumel branch near the trailing edge. The details of the mounting technique were not anticipated to be important, as the high termal conductivity copper was chosen as the plate material to ensure a uniform temperature throughout any of the plate segments. However, to provide a check on temperature uniformity, one of the central segments is equipped with an additional thermocouple mounted conventionally at the leading edge of the plate. Readings from this thermocouple agreed consistently with the alternatively mounted thermocouple, indicating that the plate temperature was uniform for the operating conditions encountered.

All the thermocouples in the flat plate model use a reference thermocouple junction placed in the flowing medium upstream of the heated plate. Thus, the thermocouple potentials are proportional to

the temperature differences between the free stream flow and the heated plates. These thermocouple potentials are measured with a sensitive voltmeter with an error less than .5° F.

A true RMS voltmeter is used to measure the AC voltage across either of the central segment heaters. This measurement, coupled with the known heater resistance is used to calculate the power consumed by the central heaters. Considering the combined accuracy of the measurements involved, the calculated power consumption is accurate to an estimated 5%.

The mass flow rate through the channel is determined simply by weighing the net mass output from the channel in a fixed time interval, usually taken to be 10 seconds. The mass flow rate is then converted to velocity using the flowing density of the material and the known channel cross-sectional area. This process was checked by comparing photographically determined particle velocities at the channel walls with velocities derived from mass flow rate data. The difference between these two velocities was generally less than 10%.

4. Experimental Procedure

After initiation of the flow, the heater power was adjusted to achieve a temperature difference between the plates and the free stream of 15 to 50° F. A steady state was reached in three to five minutes, after which the bias resistors were adjusted so that all six plate segments were at the same temperature, ± 5° F. During this process, usually taking about 10 minutes, the supply hopper was

refilled as required, the refilling being accomplished without altering the mass flow rate.

Once the plate segment temperatures were equalized within the desired tolerances, the mass flow rate, heater voltage, and plate temperatures were recorded. The flow valve was then changed to another setting and the temperature balancing process repeated.

To obtain data at higher material velocities, the area-reducing inserts were installed. The mass flow rates were selected so that the range of velocities encountered with the inserts in place overlapped the velocity range for the full channel section. In this way, any direct influence of the inserts on the data could be detected.

The short-term repeatability of the experiment was examined during a given series of measurements by alternately increasing and decreasing the mass flow rate to cover the velocity range several times. The long-term repeatability was tested by subjecting some of the materials to an additional limited series of experiments several days after the original series of tests were conducted.

5. The Materials Investigated

Four materials were selected for the experimental investigation. Three of these materials consist of hard, spherical particles with a narrow distribution of diameters about the mean. A fourth material, a common fine-grained sand, has irregularly shaped particles of relatively non-uniform size.

To express the experimental results in the dimensionless form given in (22), the thermal conductivity, thermal diffusivity, mean particle diameter, and the flowing density of the materials must be determined. The tests used to determine these properties are discussed in Appendix B, the results of these tests being summarized in Table B 1 located at the end of Appendix B.

These materials, used in conjunction with the flow channel and flat plate model previously described, produce the following approximate ranges of values for the dimensionless independent variables in (22): $k_g/k = .05-.14$; $L/d = 12-120$; $Pe_L = 100-9000$. The critical void ratio ϵ is essentially identical for the spherical particles. This is expected since spherical particles are geometrically similar and the critical void ratio should not depend on the absolute size of the particles. The fine-grained sand, however, with its irregularly shaped particles, does have a different void ratio.

6. Experimental Results

The experimental data are presented in terms of the average Nusselt number $\overline{Nu}_L$ ($\bar{h}L/k$) as a function of the Péclét number Pe_L (UL/α) for the various materials investigated. The data, expressed in this form, were found to be repeatable within the limits of the ±5% experimental scatter encountered.

In Figure 22, $\overline{Nu}_L$ versus Pe_L data are shown for the two types of glass beads and the fine-grained sand for flow over the .6 inch plate. On this same plot is given the expected result for the flow of a continuous

material, and the experimental data differ significantly from the continuum prediction. These differences, which are relatively small at low Péclét numbers, grow considerably at higher Péclét numbers. This divergence, qualitatively similar to the divergence observed with the discrete particle model, indicates clearly that the heat transfer is influenced by the non-continuous nature of the granular medium.

The solid lines through the data points in Figure 22 represent the function

$$\overline{Nu}_L = \frac{1}{\gamma + \frac{\sqrt{\pi}}{2}\sqrt{\frac{1}{Pe_L}}} \tag{23}$$

where γ is a dimensionless parameter assigned a constant value for each solid curve. This constant is selected to provide the best fit of (23) to the experimental data. For the range of the experimental data considered, this function adequately describes the Péclét number dependence of the Nusselt number, and thus γ generally will be some function of the remaining variables in (22), namely, k_g/k, L/d and ϵ. The determination of this function may be simplified by noting that the function (23) is identical in form to the numerically approximate formula discussed earlier to describe the heat transfer from a constant temperature plate with a thermal conductance K at the plate surface[1], i. e.,

$$\overline{Nu}_L = \frac{1}{\frac{k}{KL} + \frac{\sqrt{\pi}}{2}\sqrt{\frac{1}{Pe_L}}} \tag{24}$$

---

[1] This formula was given earlier in the equivalent form

$$\frac{\overline{Nu}_L}{KL/k} = \frac{1}{1+(\sqrt{\pi}/2)\beta} \quad \text{where} \quad \beta = \frac{KL}{k}\sqrt{\frac{1}{Pe_L}}$$

This correspondence suggests that γ might be given a physical interpretation, that is, $\gamma = k/KL$, where in the actual flow of particles the "effective" K is due to the presence of the relatively poor-conducting interstitial air in the irregularly shaped region between the plate surface and the first row of particles. If such an interpretation is correct, this conductance K should not depend on the heated length L of the plate. Thus, if a particular material used with a plate of length L has associated with the heat transfer data a certain γ, then this material when flowed over a plate of length L', should yield heat transfer data represented by the same function (23) with γ replaced by $\gamma' = \gamma L/L'$. In Figure 23 are shown data for the same materials as in Figure 22, but for the 1 inch length heated plates. The γ's associated with the solid lines of Figure 23 are derived from the γ's of Figure 22 by multiplying by .6. The agreement of the solid curves in Figure 23 with the data is good, supporting the proposed physical interpretation of γ. Figure 24 shows two curves corresponding to the different length plates for mustard seed, this low diffusivity material covering a relatively high range of Péclét numbers. For these data the γ's associated with the different length plates are again in the ratio .6.

Given that there is some sort of effective thermal conductance at the plate surface that is independent of the plate length, it remains to examine how this conductance varies with the properties of the granular medium. With the notion that the conductance is due to the thermal interaction between the wall and the first row of particles, it follows that for a particular set of particles, the conductance should be

proportional to the conductivity of the interstitial gas k_g, provided that heat conduction through the physical contacts and thermal radiation across the voids are a negligible portion of the total heat transferred. Furthermore, with the same assumptions, the conductance K should be inversely proportional to the average thickness of the gas film between the heated plate and the particles. Noting that this average thickness, for geometrically similar particles at the same void ratio, is proportional to the particle characteristic length d, it is postulated that

$$K = \frac{1}{\chi} \frac{k_g}{d} \tag{25}$$

where χ is a dimensionless proportionality constant which is independent of the thermal properties of the interstitial gas or the particles. This χ may be interpreted as the ratio of the thickness ℓ of a uniform gas film, with a conductance $K = k_g/\ell$, to the particle characteristic length d. For geometrically similar arrangements of particles at the plate surface, χ should, by purely dimensional reasoning, have the same numerical value. However, any changes in physical conditions which might affect the local geometrical arrangement of particles near the wall will generally change χ. For example, the use of a rough plate as opposed to a smooth one, or the use of irregularly shaped particles instead of spherical particles will affect the local particle geometry and the resultant χ will not necessarily be the same for these cases.

The validity of (25) must, of course, be verified by experimental data. To examine the verifiable consequences of (25), substitution of this relationship into (24) yields

$$\overline{Nu}_L^* = \frac{1}{\chi + \frac{\sqrt{\pi}}{2}\sqrt{\frac{1}{Pe_L^*}}} \tag{26}$$

where

$$\overline{Nu}_L^* = \frac{k}{k_g}\frac{d}{L}\overline{Nu}_L = \frac{\bar{h}d}{k_g}$$

and

$$Pe_L^* = \left(\frac{k}{k_g}\right)^2\left(\frac{d}{L}\right)^2 Pe_L$$

Thus, it follows from (25) that the heat transfer data for geometrically similar particle arrangements, such as occurs with spherical particles flowing over a smooth plate, should lie on a single curve with the modified Nusselt number $\overline{Nu}_L^*$ and Péclét number Pe_L^* as coordinates. In Figure 25, all the spherical particle data are shown using this modified coordinate system, and the data do in fact lie on a single curve with a good degree of correlation. Furthermore, this single curve is well represented by the function (26) with $\chi = .085$, i.e., for an "effective" air film thickness about 1/10 of a particle diameter. The data for the fine-grained sand, with its irregularly shaped particles, lies distinctly below the spherical particle data. This difference is consistent with the physical interpretation of the wall conductance discussed above; the sand, with its irregularly shaped particles and different void ratio should not necessarily have the same χ.

D. Discussion and Concluding Remarks

The experimental data presented shows that the treatment of granular media consisting of spherical particles as effectively a continuum with a thermal conductance K at the wall leads to a reasonable correlation for the heat transfer from the flat plate immersed in a granular flow. A major consequence of this correlation is that substantial deviation from the heat transfer rates predicted assuming the granular media to be continuous can occur, the severity of this deviation being a function of a single dimensionless group, the modified Péclét number

$$Pe_L^* = \left(\frac{d}{L}\right)^2 \left(\frac{k}{k_g}\right)^2 Pe_L .$$

The empirical formula used for the correlation of experimental data was motivated by experience with the discrete particle model; the exact analytical prediction of the heat transfer from a flat plate in a discrete particle flow was found to be reasonably approximated by treating the medium as a continuum with a single conductance at the plate surface. It is important to point out, however, that the approximation to the analytical solution for discrete particle flows and the empirical correlation, while similar, are not identical. The difference lies in the numerical choice of the conductance at the plate surface. In the discrete particle model this conductance is given by k/d, a choice which is appropriate for infinitely conducting particles in the regular array associated with the model. Since in an actual flow the particles are neither infinitely conducting nor regularly arranged, the direct use

of the formula $K = k/d$ does not lead to the most suitable correlation. Instead, the choice, made on physical grounds, of K proportional to k_g/d was found to be more accurate, and this formula was used in the final correlation. The differences in the conductance calculated with these alternative formulas are the order of 25% for the sand and glass beads, and 50% for the mustard seed (this material has the poorest conductivity of the materials tested). Aside from these numerical deviations, however, the discrete particle model behaves qualitatively like the materials tested.

The correlation that has been presented for spherical particle heat transfer from the flat plate cannot be applied, of course, outside of the restrictions implied by the assumptions made in the preceding development. For example, as was pointed out in Section C 1 on dimensional analysis, it is required to ensure negligible particle to particle heat transfer by thermal radiation that

$$\frac{\sigma T^3 d}{k_g} < .5 ,$$

where T is the absolute temperature of the flat plate[1]. The direct application of the $Nu_L^* - Pe_L^*$ relationship given here to systems where the ratio $\sigma T^3 d/k_g$ is larger than .5 could lead to substantial error. Another factor omitted in the analysis was the ratio of the interstitial gas heat capacity per unit volume to that of the particles. This variable

[1] For the experiments discussed, the largest value of $\sigma T^3 d/k_g$ is approximately .2, this value occurring with the mustard seed at a plate temperature of 125° F.

was neglected because of the tendency of a low density interstitial gas surrounded by relatively high density particles to behave quasi-statically, except near the leading edge of the plate. For the assumption of negligible gas heat capacity to be reasonable, the "entry length" $\mathcal{L}$ of the plate, that is, the portion of the plate from the leading edge to a position $x = \mathcal{L}$ where the gas does not behave quasi-statically, must be small compared to the total plate length L. Recall from Section C 1 that for a gas film of thickness ℓ adjacent to the plate surface, the entry length $\mathcal{L}$ is given by the relation

$$\frac{\mathcal{L}}{\ell^2} \frac{\alpha_g}{U} = .5 .$$

Taking ℓ to be d/10, the value of the effective film thickness found experimentally, the requirement that the entry length be small may be expressed as

$$\frac{\mathcal{L}}{L} = .005 \frac{d^2}{L} \frac{U}{\alpha_g} = .005 \left(\frac{d}{L}\right)^2 \frac{\alpha}{\alpha_g} Pe_L$$

$$= .005 \, Pe_L^* \frac{k_g \rho_g c_g}{k \rho c} << 1 .$$

For the tests conducted in this paper, the maximum value of $\mathcal{L}/L$ occurs with the mustard seed at high Péclét numbers and is approximately .002. In view of this small value, therefore, the heat capacity of the air should be effectively negligible. However, the use of the correlation presented for modified Péclét numbers substantially higher than those covered in the experiments should be done with care, as the heat capacity of the interstitial fluid may influence the results.

The nature of the heat transfer from the flat plate differs considerably depending on the magnitude of modified Péclét numbers encountered. For low modified Péclét numbers, $Pe^{*}<2$, the granular material functions as a single component continuum and the heat transfer from the flat plate is governed solely by the bulk thermal properties k and α. Those properties characterizing the structure of the granular material, that is, the particle diameter and gas conductivity, have no direct influence on the heat transfer for these low modified Péclét numbers. For large values of the modified Péclét number (greater than 1000), the heat transfer is dominated by the thermal resistance at the wall; as a result the film coefficient is close to being inversely proportional to the particle diameter and directly proportional to the interstitial gas conductivity. In between these two extremes of modified Péclét number is a large transitional regime where both the bulk and structural properties of the medium influence the heat transfer. The notion of two different heat transfer regimes corresponding to the continuous or non-continuous behavior of granular materials can be used to explain the dichotomy previously discussed with regard to the data of Brinn, et al [3] and Kurochkin [4]. In Brinn's experiments with fine-grained materials flowing through tubes, the maximum modified Péclét number encountered (based on the tube length and average particle diameter), is approximately 4, and thus any non-continuum effects would be small and difficult to detect through the experimental scatter. Unfortunately, Kurochkin does not provide sufficient data to calculate the modified Péclét number based on the flow length of the

geometries investigated. However, since [4] reported that the film coefficient is inversely proportional to the particle diameter, it is likely that the modified Péclét numbers associated with these data are substantial, and the heat transfer is dominated by the thermal conductance at the body surface. In the study of Harakas and Beatty [5], the bulk of their data corresponds to low modified Peclet numbers and the continuum behavior observed by these investigators is consistent with the results given here. There are in [5] some data for glass beads corresponding to modified Péclét numbers in the range 10-50 which differ somewhat from the proposed correlation. This disagreement is believed to be due to differences in the thermal property measurements.

The data shown here for the fine-grained sand, with its irregularly shaped particles and relatively high void ratio, deviates slightly from the universal curve proposed for spherical particles. This is believed to be due to the difference, compared to spherical particles, in the geometry of the particle-wall interaction. The trend of the data for sand indicates, however, that the results may still be described with the same concept applied for spherical particles, although a different magnitude wall conductance is required. More data at higher modified Peclet numbers are needed to confirm this contention.

A study of heat transfer from more complicated shapes has not been conducted here, but it appears plausible that the notion of an effective thermal conductance along the surface of the body in contact with the flowing material should apply. Furthermore, the conductance should not differ substantially from that observed in the flat plate

experiments. Thus, the data here may be used to estimate the heat transfer from more complicated shapes either by applying a flow theory or physical observation to determine the velocity field about the body and solving the convective energy equation with the appropriate thermal resistance at the wall surface.

REFERENCES

[1] Uhl, V. W. and Root, W. L., "Heat Transfer to Granular Solids in Agitated Units", Chemical Engineering Progress, vol. 63, no. 7, July 1967, pp. 81-92.

[2] Kramer, R. L., Director of Engineering Development, The Procter & Gamble Company, Private Communication.

[3] Brinn, M. S., et al, "Heat Transfer to Granular Materials", Industrial and Engineering Chemistry, vol. 40, no. 4, June 1948, pp. 1050-1061.

[4] Kurochkin, Yu. P., "Heat Transfer Between Tubes of Different Sections and a Stream of Granular Material", Journal of Engineering Physics, vol. 10, no. 6, 1966, pp. 447-449.

[5] Harakas, N. K. and Beatty, K. O., "Moving Bed Heat Transfer: Effect of Interstitial Gas with Fine Particles", Chem. Engineering Progress Symposium Series, vol. 59, no. 41, pp. 122-128.

[6] Jenike, A. W., Elsey, P. J. and Woolley, R. H., "Flow Properties of Bulk Solids", Proceedings, ASTM, vol. 60, 1960, pp. 1168-1181.

[7] Pariseau, W. G., "Gravity Flow of Ideally Plastic Materials through Slots", Transactions, ASME, Journal of Engineering for Industry, vol. 91, May 1969, pp. 414-422.

[8] Roscoe, K. H., Schofield, A. N. and Wroth, C. P., "On the Yielding of Soils", Geotechnique, vol. 8, 1958, pp. 22-53.

[9] Jenike, A. W. and Shield, R. T., "On the Plastic Flow of Coulomb Solids Beyond Original Failure", Transactions, ASME, Series E, vol. 81, 1959, pp. 599-602.

[10] Scott, R. F., "Principles of Soil Mechanics", Addison-Wesley Publishing Company, Inc., 1963, Chapter 9.

[11] Ibid., Chapter 5.

[12] Spencer, A. J. M., "A Theory of the Kinematics of Ideal Soil under Plane Strain Conditions", J. Mech. Phys. Solids, vol. 12, pp. 337-351.

[13] DeJosselin De Jong, G., "Statics and Kinematics in the Failable Zone of a Granular Material", Ph.D. Thesis, Laboratorium de Grondmechanica of Delft, February 1959.

[14] Bingham, E. C. and Wikoff, R. W., "The Flow of Dry Sand through Capillary Tubes", Journal of Rheology, vol. 2, no. 4, October 1931, pp. 395-401.

[15] Wieghardt, V. K., "Ukereinige Versuche on Stromungen in Sand", Ingenieur-Archiv, vol. 20, 1952, pp. 109-115.

[16] Johanson, J. R., "Method of Calculating Rate of Discharge from Hoppers and Bins", Transactions of the Society of Mining Engineers, vol. 232, March 1965, pp. 69-80.

[17] Johanson, J. R., "Stress and Velocity Fields in Gravity Flow of Bulk Solids", Ph. D. Thesis, University of Utah, 1962.

[18] Jenike, A. W., "Steady Gravity Flow of Frictional Cohesive Solids in Converging Channels", Journal of Applied Mechanics, vol. 31, Transactions, ASME, vol. 84, Series E, 1964, p. 5-11.

[19] Gröbner, W. and Hofreiter, N., "Interraltafel", Springer-Verlag, 1949.

[20] Carslaw, H. S. and Jaeger, J. C., "Conduction of Heat in Solids", 2nd ed., Oxford University Press, 1959, p. 75.

[21] Ibid., p. 74.

[22] Yagi, S. and Kunii, D., "Studies on Heat Transfer Near Wall Surface in Packed Beds", A. I. Ch. E. Journal, vol. 6, 1960, pp. 97-104.

[23] Yagi, S. and Kunii, D., "Studies on Effective Thermal Conductivities in Packed Beds", A. I. Ch. E. Journal, vol. 3, no. 3, pp. 373-381.

[24] Schotte, W., "Thermal Conductivity of Packed Beds", A. I. Ch. E. Journal, vol. 6, pp. 63-67.

[25] Wechsler, A. E. and Glaser, P. E., "Pressure Effects on Postulated Lunar Materials", Icarus, vol. 4, 1965, pp. 335-352.

[26] Kreith, F., "Principles of Heat Transfer", 2nd ed., International Textbook Company, 1967, pp. 166-175.

APPENDIX A

HEAT LOSS ESTIMATES

In the experimental work presented in this report, the film coefficients are calculated assuming that, under steady state conditions, essentially all the heat added to the central plate segment is removed by the flow of granular material. For such an assumption to be reasonable, it is required that the heat transferred from the central plate segments to portions of the apparatus other than the flow field are a small fraction of the net heat added to the plate. In this appendix, the magnitude of these losses will be estimated to check the legitimacy of assuming that all the power supplied to the plate is directly transferred to the granular material. The major losses to be considered here are due to heat conduction from the central plate segment to the plexiglass plate holder or to the outer plate segments.

The heat loss from the central plate to the plate holder occurs by conduction across the air gaps located at the leading and trailing edges of the central plate. In the following calculation, the heat transferred through the thin cellophane tape covering the air gap shall be neglected, and it will be assumed, conservatively, that the plexiglass holder is at the free stream temperature T_{oo}. Referring to Figure A-1, the heat transfered per unit time through both air gaps is given by

$$q_{\ell 1} = 2twk_a \frac{\Delta T}{\ell}$$

where $\Delta T = T_w - T_\infty$ is the temperature change across the gap and k_a the conductivity of air. The total heat added to the central plate is, using the definition of the film coefficient $\bar{h}$,

$$q_t = Lw\bar{h}\Delta T$$

Thus, the ratio

$$R_1 = \frac{q_{\ell 1}}{q_t} = \frac{2tk_a}{\ell L\bar{h}}$$

represents the fraction of heat added to the plate which is lost to the plexiglass holder. For the experimental system used here, the maximum value of this ratio occurs with the mustard seed, where film coefficients as low as 15 Btu/hr-ft^2-°F were encountered using the .6" length plate. Noting that $k_a = .015$ Btu/hr-ft-°F, $t = 1/16"$, and $\ell = 1/16"$, the largest value of R_1 is found to be

$$R_1 = 2\left(\frac{1/16}{1/16}\right)\frac{12}{.6}\left(\frac{.015}{15}\right) = .04 = 4\%.$$

The second major source of heat loss results from the inability to exactly equalize the temperatures of the outer guard segments and the central segments. This loss, for a temperature difference ΔT_g between the central and outer plate segments is given by

$$q_{\ell 2} = \frac{2tLk_a}{g}\Delta T_g$$

and thus the ratio of this loss to the total heat added is

$$R_2 = \frac{q_{\ell 2}}{q_t} = 2\left(\frac{t}{g}\right)\left(\frac{k_a}{\bar{h}w}\right)\frac{\Delta T_g}{\Delta T} .$$

The maximum value of this ratio, calculated from experimental measurements of ΔT_g, ΔT and $\bar{h}$ is approximately 2.5%.

Thus, the total calculated losses, for the most unfavorable operating conditions, amount to approximately 6% of the heat supplied. This loss, which is the order of the experimental scatter encountered, is considered to be essentially negligible.

APPENDIX B

PHYSICAL PROPERTY MEASUREMENTS

The physical properties of the granular materials required for the data reduction scheme used in this thesis are the average particle size, material density, void ratio, thermal diffusivity, and thermal conductivity. With the exception of particle size, the properties desired are "bulk" quantities, that is, they reflect an average material response resulting from the individual contributions of many particles. Thus, the measuring equipment to be described is designed with characteristic lengths much larger than the particle size of the materials investigated.

A given granular material is capable of assuming a range of void ratios corresponding to the more or less dense packing of the particles, and generally the bulk properties of density, thermal diffusivity, and conductivity will be functions of the void ratio. The properties required in the experimental correlations, however, refer to the material in a flowing state, and therefore bulk property determinations are made here at the critical void ratio. For completeness, data for more densely packed states are also given, although this information is not utilized in the heat transfer experiments.

In the following paragraphs, the specific methods used for determining the properties are described. The results of the tests are summarized in Table B-1 at the end of the appendix.

Particle Size

The materials investigated contain particles which are generally not uniform in size or shape, and thus the term "particle size" refers to some appropriate average characteristic length of the particles. The characteristic length used here is defined as the distance between two parallel planes adjusted so that each plane is tangent to opposite sides of the particle being meausred. This length is chosen since its measurement is easily effected using a microscope with a special eyepiece inscribed with two vertical lines, the distance d between the lines being adjustable and measurable with a micrometer dial. For the case of spherical particles, d is simply the particle diameter, while for irregularly shaped particles, such as those found in the fine-grained sand, the characteristic length depends on the specific orientation of the particle. However, since measurements are made for many particles with random orientation, the average characteristic length should be a reasonable measure of the particle size.

The experimental procedure consists of pouring a sample of granular material onto a microscope slide, slowly traversing the slide with the microscope objective, and measuring any particle entering the field of view. For each material tested, measurements were made on the order of 100 particles. The results of these measurements, in terms of particle size histograms, are shown in Figures B-1 through B-3.

Bulk Density and Void Ratio

The bulk density is determined simply by measuring the volume, with a large graduate cylinder, of a known mass of granular material. The volume corresponding to the critical void ratio is obtained by capping the end of the graduate cylinder and flowing the material by slowly inverting the cylinder. Denser states are realized by repeated striking of the cylinder, until no further compaction of the material is observed.

The void ratio, defined as the ratio of the void volume to the solid particle volume in a uniform sample of granular material, may be calculated from the known bulk density ρ of the granular material and the particle density ρ_p with the formula[1]

$$\epsilon = \frac{\rho_p}{\rho} - 1$$

To determine ρ_p, a given granular sample is weighed in air, then in water, and the following equality, derived assuming the interstitial air is completely displaced by the water, is used:

$$\frac{W_{wat} + B}{W_{air}} = \frac{\rho_p - \rho_{wat}}{\rho_p}$$

In this formula, W_{air} is the weight of the sample in air, W_{wat} the weight of the same sample in water, and B the bouyancy of the particle container.

---

[1] This formula assumes that the mass of air in the voids is negligible compared to the solid mass.

Thermal Diffusivity

It was decided to use the unsteady state approach outlined by Brinn, et al [1][1] to directly measure the diffusivity of the materials investigated. This technique, to be described below, has the advantage of experimental simplicity and relatively short data collection time.

The principal component of the apparatus is a long, 1-1/2 inch diameter hollow copper cylinder, shown in Figure B-4. Two chromel-alumel thermocouples, one suspended at the center of the cylinder, and the other imbedded in the cylinder walls, are used for temperature measurements. An electrical heating tape is tightly wrapped around the cylinder and energized with an adjustable voltage source.

The experimental procedure begins with quickly raising the copper cylinder temperature to some T_1 which is the order of 50°F above the initial, uniform temperature of the system. As time proceeds, the power supplied to the tape is adjusted so that the cylinder wall remains at temperature T_1, within a tolerance of 1/2 °F. At regular intervals, usually every minute, the temperature T_c of the granular material at the center of the cylinder is recorded, using a sensitive microvoltmeter.

It is shown in [2] that for a cylinder initially at the uniform temperature T_0 with a wall at radius R suddenly raised[2] to temperature

[1] Numbers in brackets designate references listed at end of Appendix B.

[2] Consideration of the problem of a linear increase in wall temperature from T_0 to T_1 in time t^*, followed by constant wall temperature thereafter, yields essentially the same results, provided the group $\alpha t^*/R^2 < .1$. For the short initial heating times used in these experiments, $\alpha t^*/R^2 < .1$, hence the experimental cylinder shall be considered to behave as if T_1 is realized instantaneously.

T_1 at time $t = 0$, the center temperature is given by

$$\theta(t) = \frac{T_1 - T_c}{T_1 - T_0} = 2 \sum_{n=1}^{\infty} e^{-\alpha(a_n^2 t/R^2)} \frac{J_0(0)}{a_n J_1(a_n)}$$

where J_0 and J_1 are the ordinary Bessel functions and a_n are the zeros of J_0, $a_1 = 2.404$, $a_2 = 5.201$, ... Noting that successive terms in this series decrease in importance as $\alpha t/R^2$ becomes large, it follows that a plot of $\log_{10} \left[T_1 - T_c / T_1 - T_0\right]$ versus t should approach a straight line with a slope of $-2.5\alpha/R^2$ for large t. By comparing the magnitude of the first and second terms in the above series, it is seen that values of $\alpha t/R^2$ greater than .3 are "large", this value being reached in the order of 10 minutes for typical granular material heated in a 1-1/2 inch diameter cylinder.

Figure B-5 shows a semi-log plot of the experimentally determined quantity $\left[T_1 - T_c / T_1 - T_0\right]$ versus time. The fact that $\log_{10} \left[T_1 - T_c / T_1 - T_0\right]$ approaches a straight line indicates that the errors associated with the measurement of T_c, due to general thermocouple inaccuracy and the inability to maintain the cylinder wall temperature at exactly T_1, are small.

Thermal Conductivity

The thermal conductivity is not measured directly in the following experiment, but rather the specific heat c of the particles. The specific heat is then used in conjunction with the previously determined bulk density ρ and diffusivity α to yield the conductivity, $k = \alpha \rho c$.

The same equipment discussed in connection with the diffusivity experiment is utilized to measure the specific heat. However, the apparatus is modified so that a boundary condition of constant heat flux at the cylinder wall is imposed, rather than the constant temperature condition used in the diffusivity experiment. To effect this change, the single strip heater adjacent to the cylinder is tightly wrapped with a 1/16 inch thick cardboard sheet followed by a similar strip heater (Figure B-6). The outermost strip heater acts as a heat guard, as the voltage across this heater is manually regulated to equalize, within a 1/2 °F tolerance, the temperatures of two thermocouples imbedded on opposite sides of the cardboard sheet. The entire cylinder is then wrapped in rock wool insulation to minimize losses from the portions of the cylinder not covered by the laminated heater system.

Data are collected by applying a measured AC voltage to the inner heater, then recording the cylinder temperature T_1 and the center temperature T_c at one minute intervals.

Neglecting for the moment the heat capacity of the copper cylinder, the exact solution to the heat diffusion equation for a constant heat flux q'' applied at the radius $r = R$ at time $t = 0$ is [3]

$$T(r,t) - T_0 = 2q'' \frac{\alpha t}{kR} + q'' \frac{R}{k}\left[\frac{r^2}{2R^2} - \frac{1}{4} - 2\sum_{n=1}^{\infty} e^{-\alpha t b_n^2/R^2} \frac{J_0(rb_n/R)}{b_n^2 J_0(b_n)}\right]$$

where $J_1(b_n) = 0$ ($b_1 = 3.832$, $b_2 = 7.016, \cdots$). For values of $\alpha t/R^2 > .5$, the terms in the infinite series are negligible compared to the term linear in time, and thus a plot of the wall temperature $T_1 - T_0$ should approach

a linear asymptote with a slope of $2q''/\rho cR$, and this slope may be used to find c.

The heat capacity of the copper cylinder, however, does have an effect on the terminal slope of the temperature-time curve, as can be shown by examining long-time solutions obtained by transform techniques. These solutions, which are algebraically complex, yield a simple, intuitively clear result for the terminal temperature-time slope when expressed in terms of the total heat Q added to the cylinder,

$$\lim_{t \to \infty} \frac{dT_1}{dt} = \frac{Q}{M_1 c_1 + M_p c}$$

where M_1 and M_p are the mass of the cylinder and granular material, respectively, and c_1 the specific heat of copper.

Figure B-8 shows a typical temperature-time plot for sand using the described apparatus. The temperature difference $T_1 - T_c$ is also shown, and this difference approaches a constant value as both temperatures converge to their linear asymptotes.

Repeated tests using different applied voltages and varying quantities of granular material in the cylinder yielded the same specific heat within a scatter of 5%.

REFERENCES
(APPENDICES)

[1] Brinn, M. S., et al, "Heat Transfer to Granular Materials", Industrial and Engineering Chemistry, vol. 40, no. 4, June 1948, pp. 1050-1061.

[2] Carslaw, H. S. and Jaeger, J. C., "Conduction of Heat in Solids", 2nd ed., Oxford University Press, 1959, p. 199.

[3] Ibid, p. 203.

TABLE B-1

	Glass Traffic Beads	Glass Impact Beads	Mustard Seed	Fine-Grained Sand
Mean Particle Size (inches)	0.013	0.053	0.085	0.008
Standard Deviation (%)	2.4	1.0	1.2	2.5
Bulk Density (specific weight)				
Critical State	1.5	1.7	.7	1.5
Dense State	1.6	1.8	.8	1.7
Void Ratio (%)				
Critical State	73.	71.	74.	91.
Dense State	60.	59.	59.	63.
Thermal Diffusivity $\times 10^6$ (ft^2/sec)				
Critical State	1.7	1.7	.9	3.1
Dense State	2.1	1.8	.9	3.3
Thermal Conductivity (Btu/hr-ft-°F)				
Critical State	.12	.11	.08	.2
Dense State	.16	.13	.09	.3

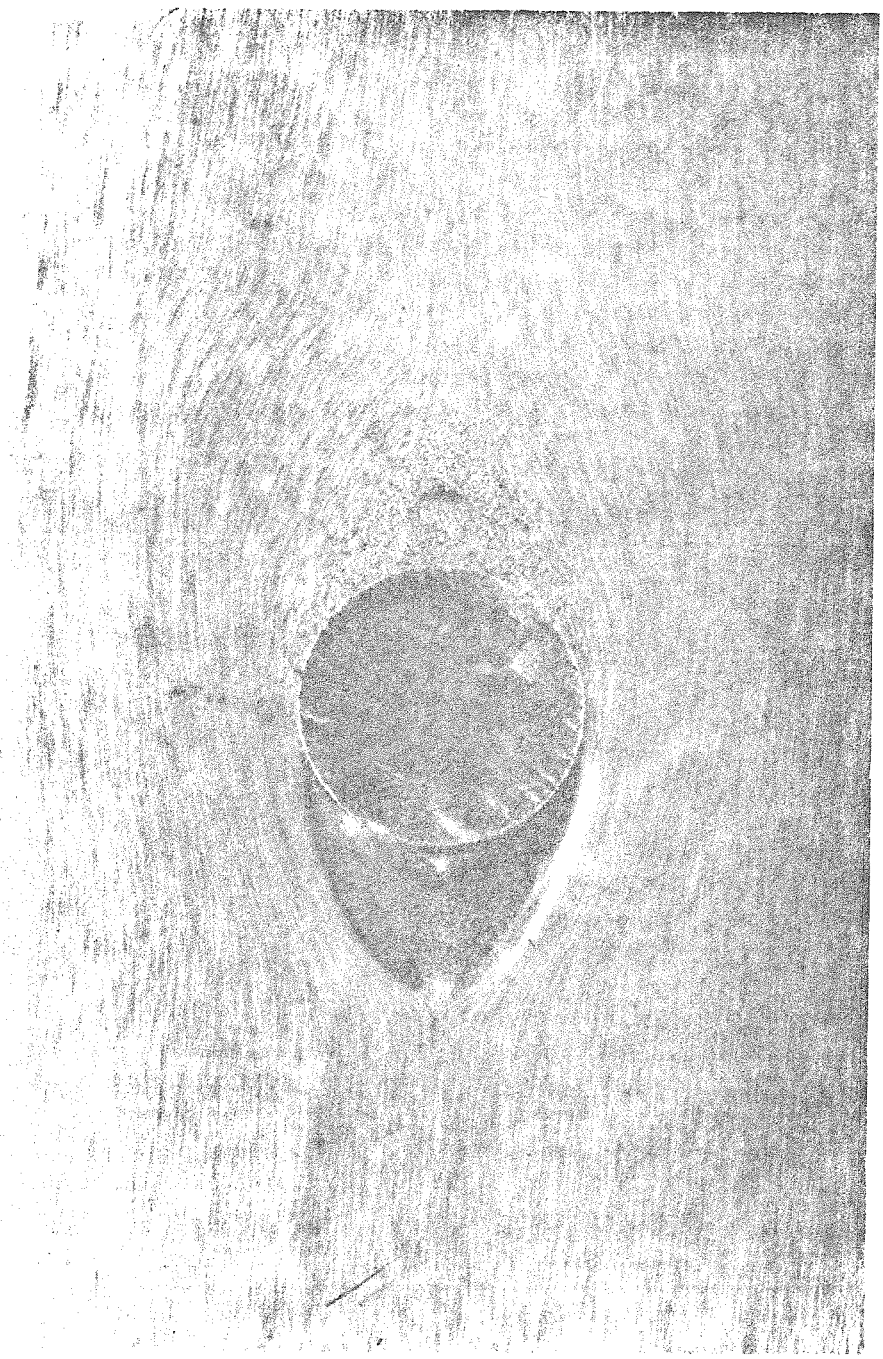

Figure 1(a) Flow of sand (top to bottom) about 1" dia. cylinder at approximately 2 inches per second.

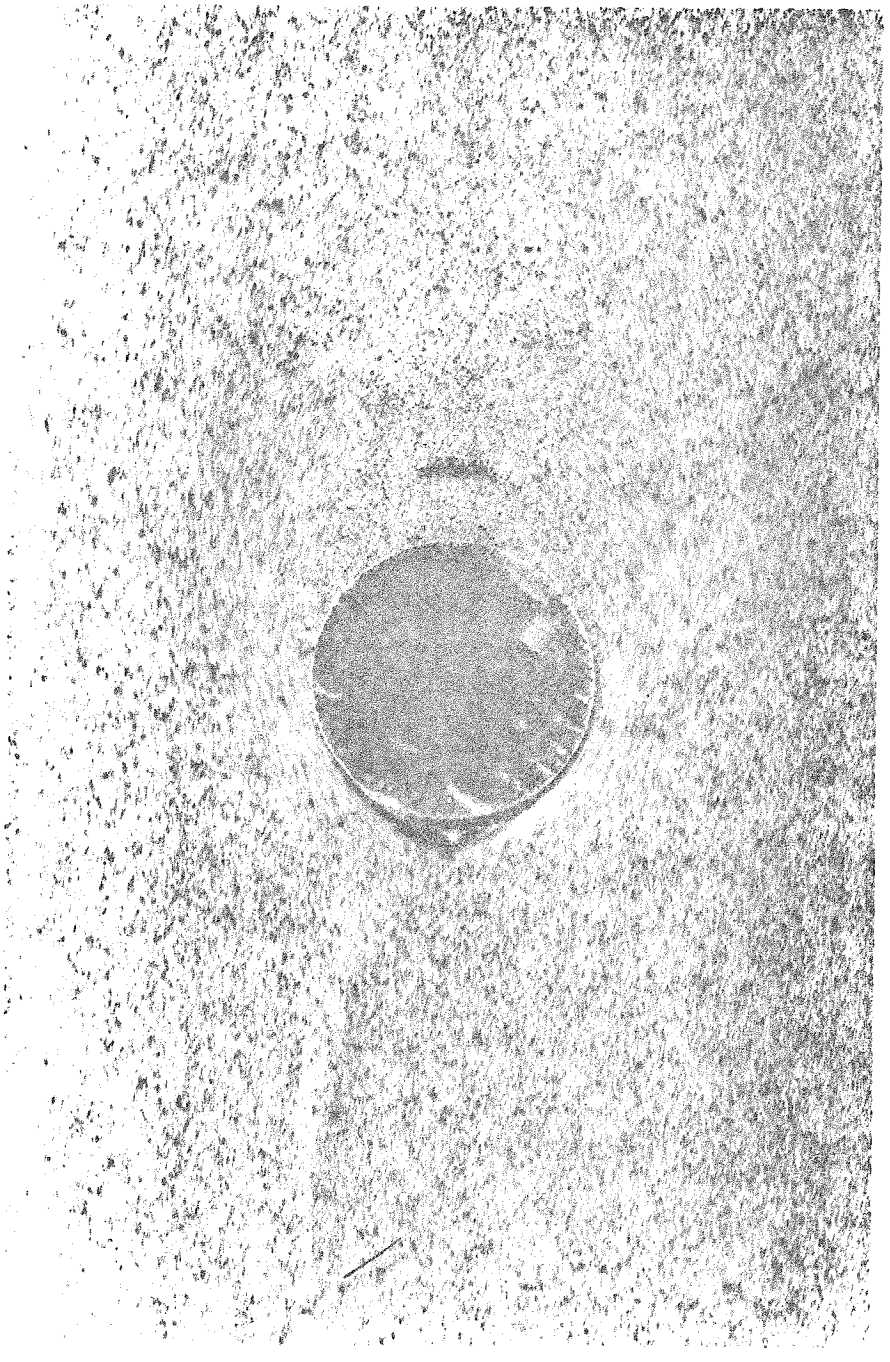

Figure 1(b) Flow of sand (top to bottom) about a 1" dia. cylinder at approximately .2 inches per second.

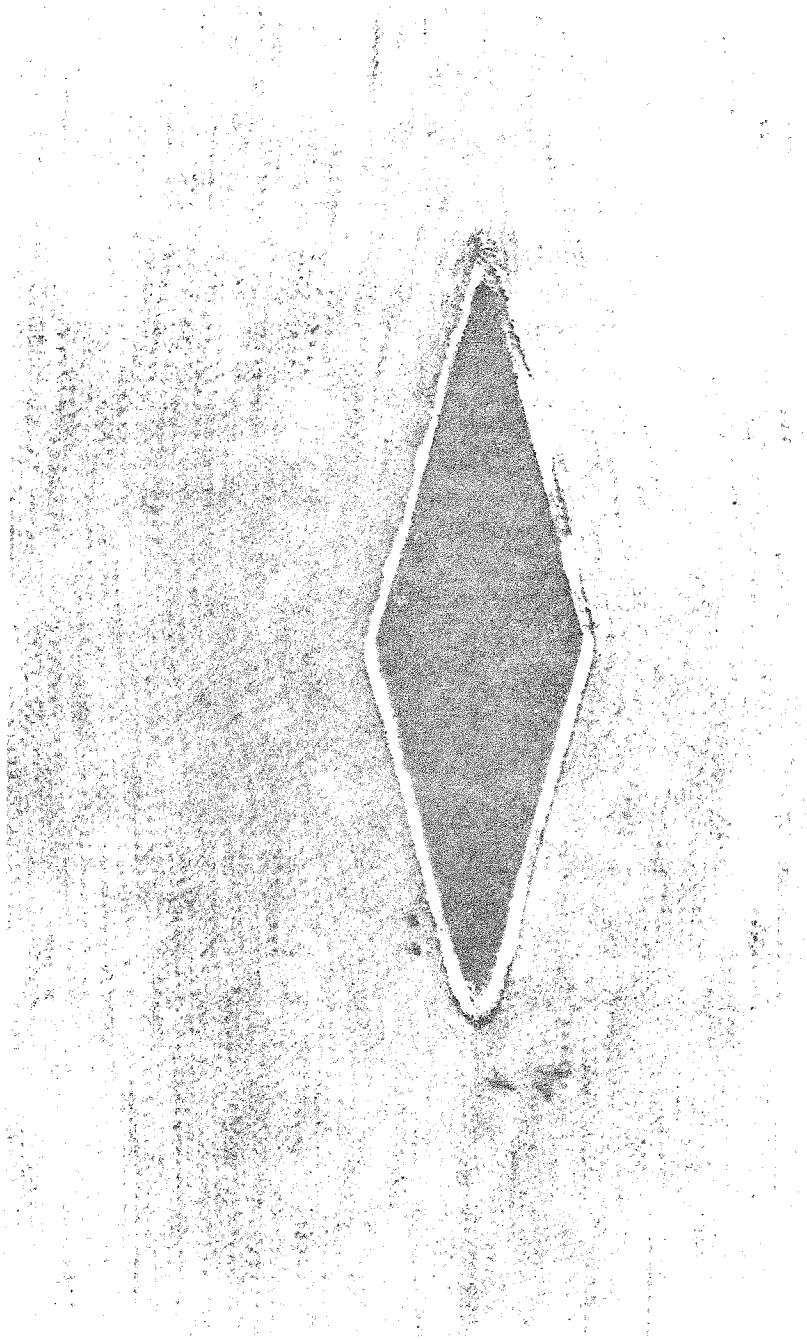

Figure 2 Flow of Sand (top to bottom) about a 1" length double wedge at approximately 2 inches per second.

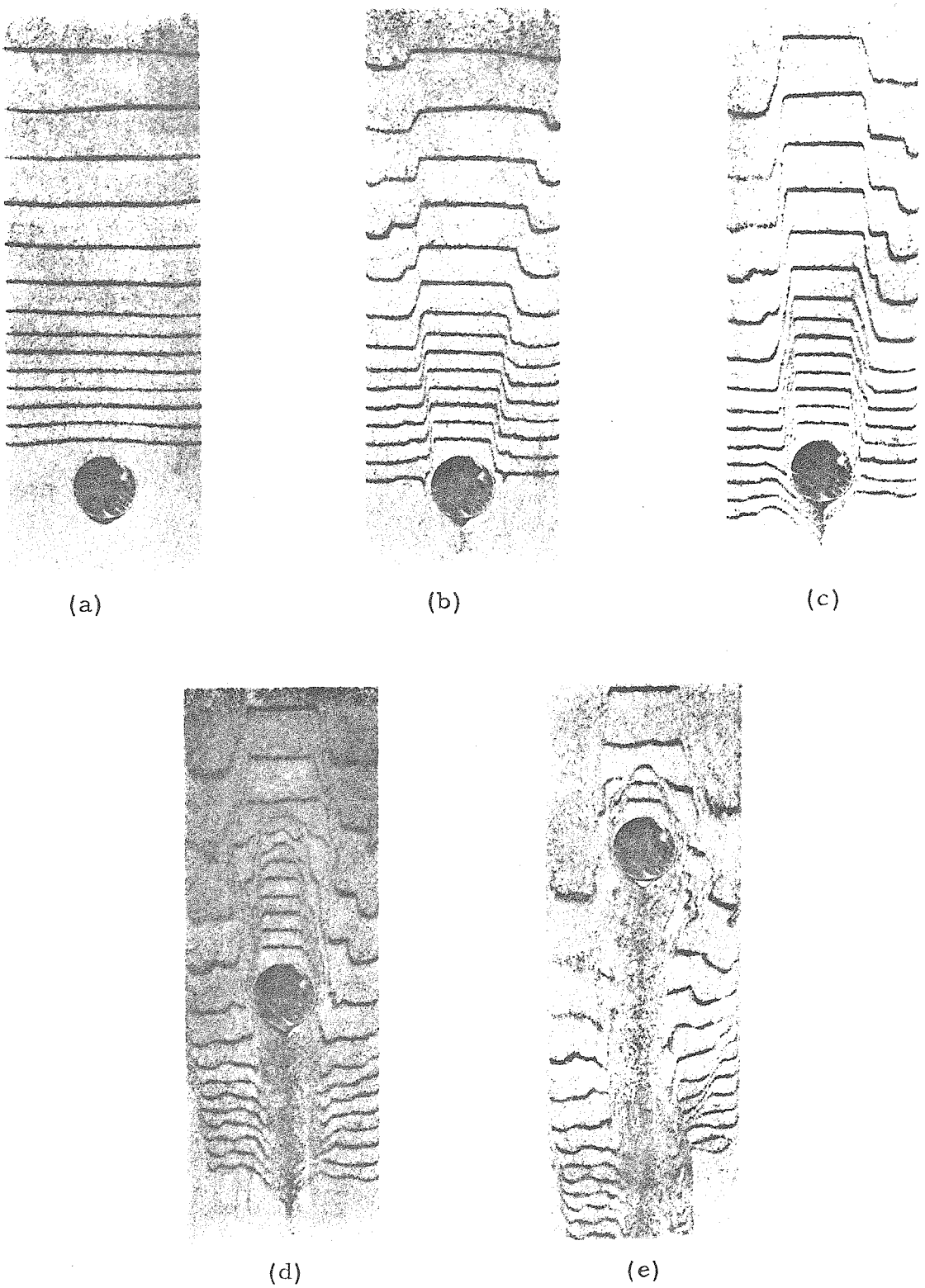

Figure 3 Development of flow about a cylinder with the sand in an initially dense state.

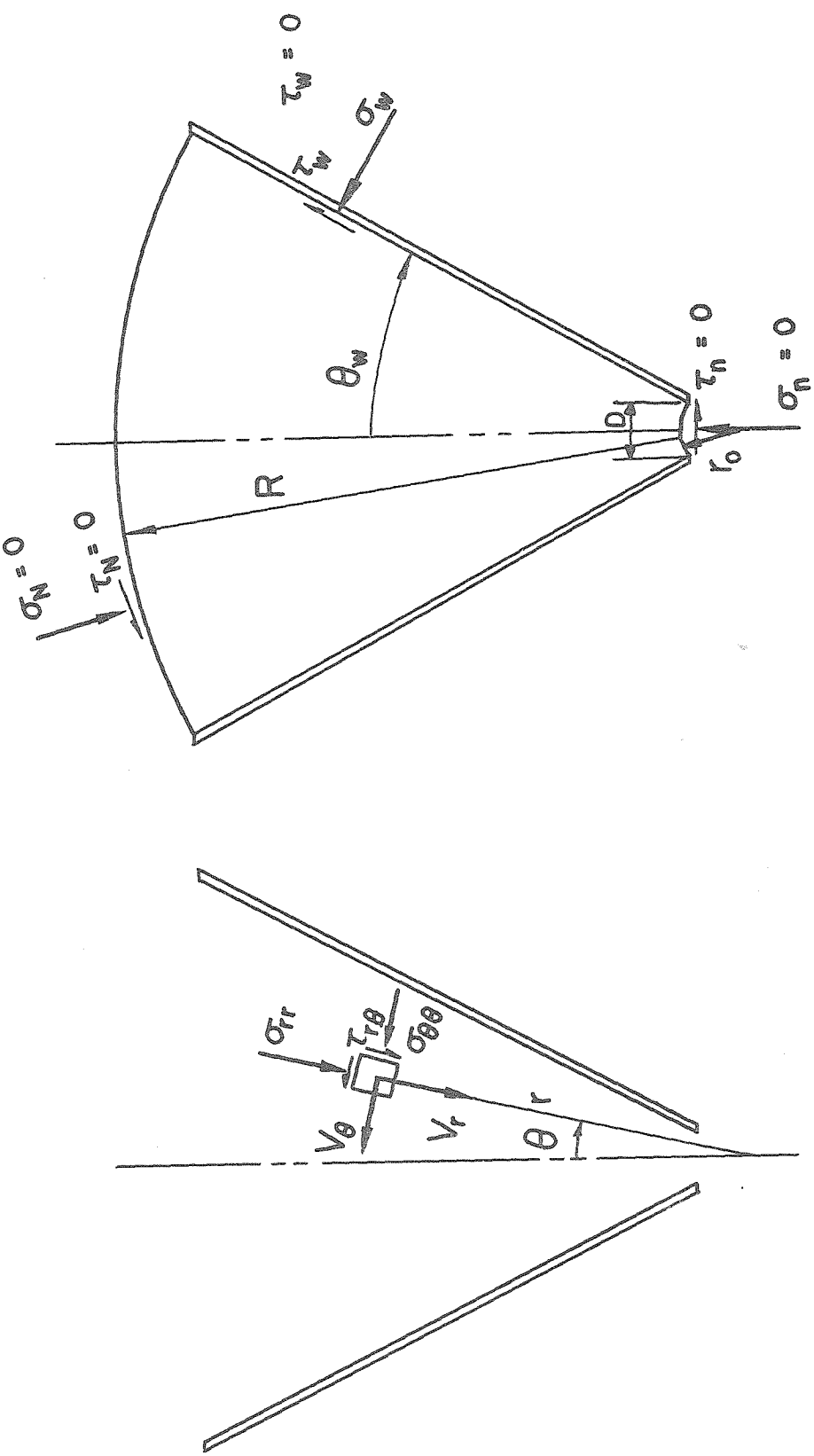

Figure 4 Converging channel with frictionless walls under the influence of a radial body force.

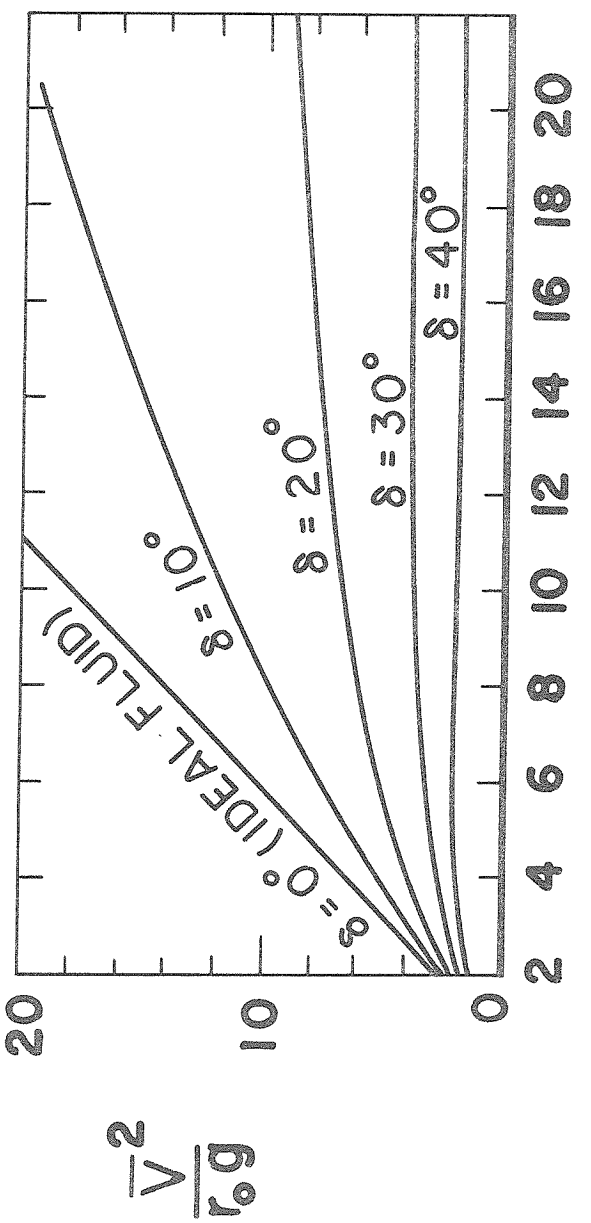

Figure 5 Efflux velocity as a function of material head above the orifice for the radial body force solution.

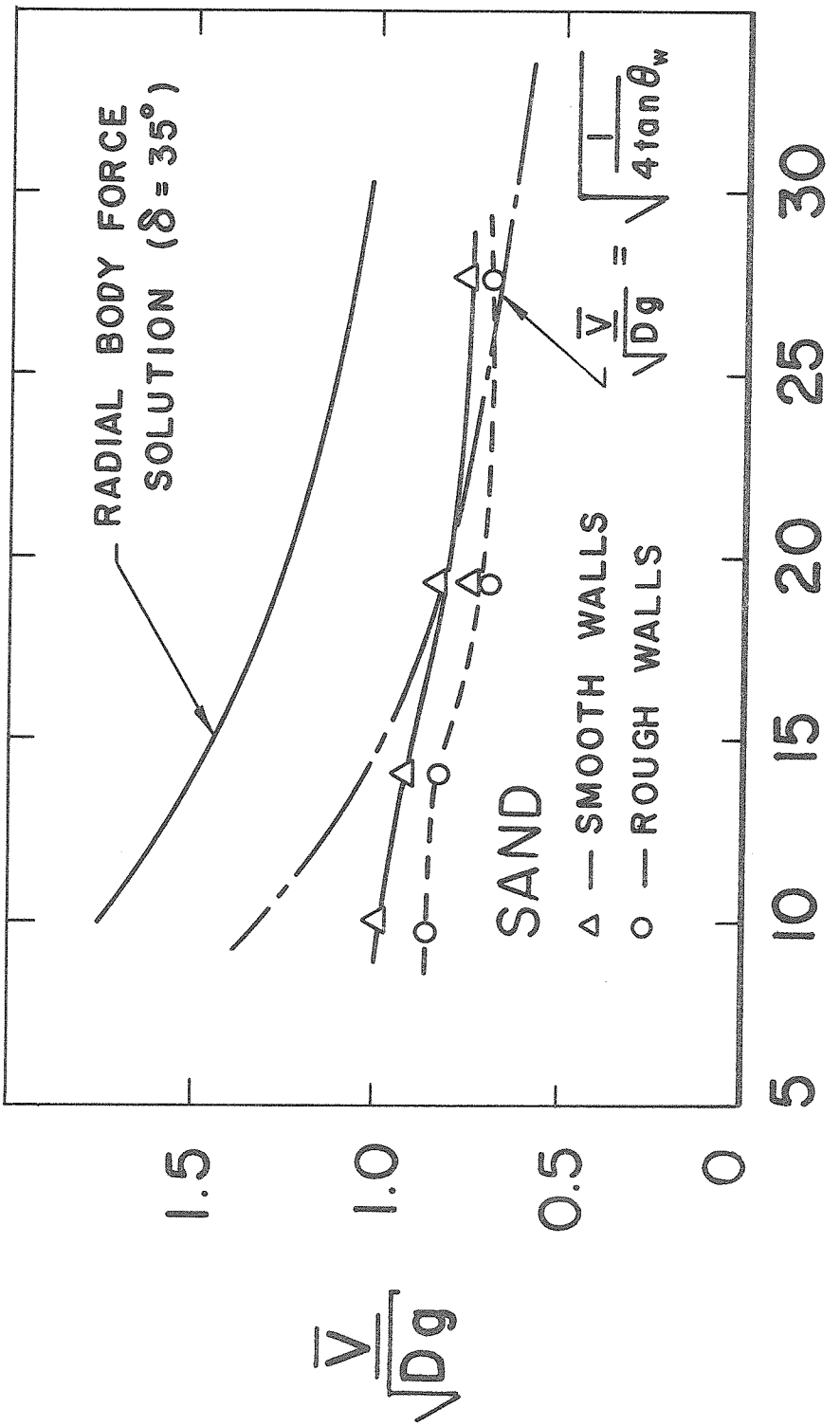

Figure 6 Dimensionless efflux velocity for sand ($\delta = 35°$) flowing through conical channels.

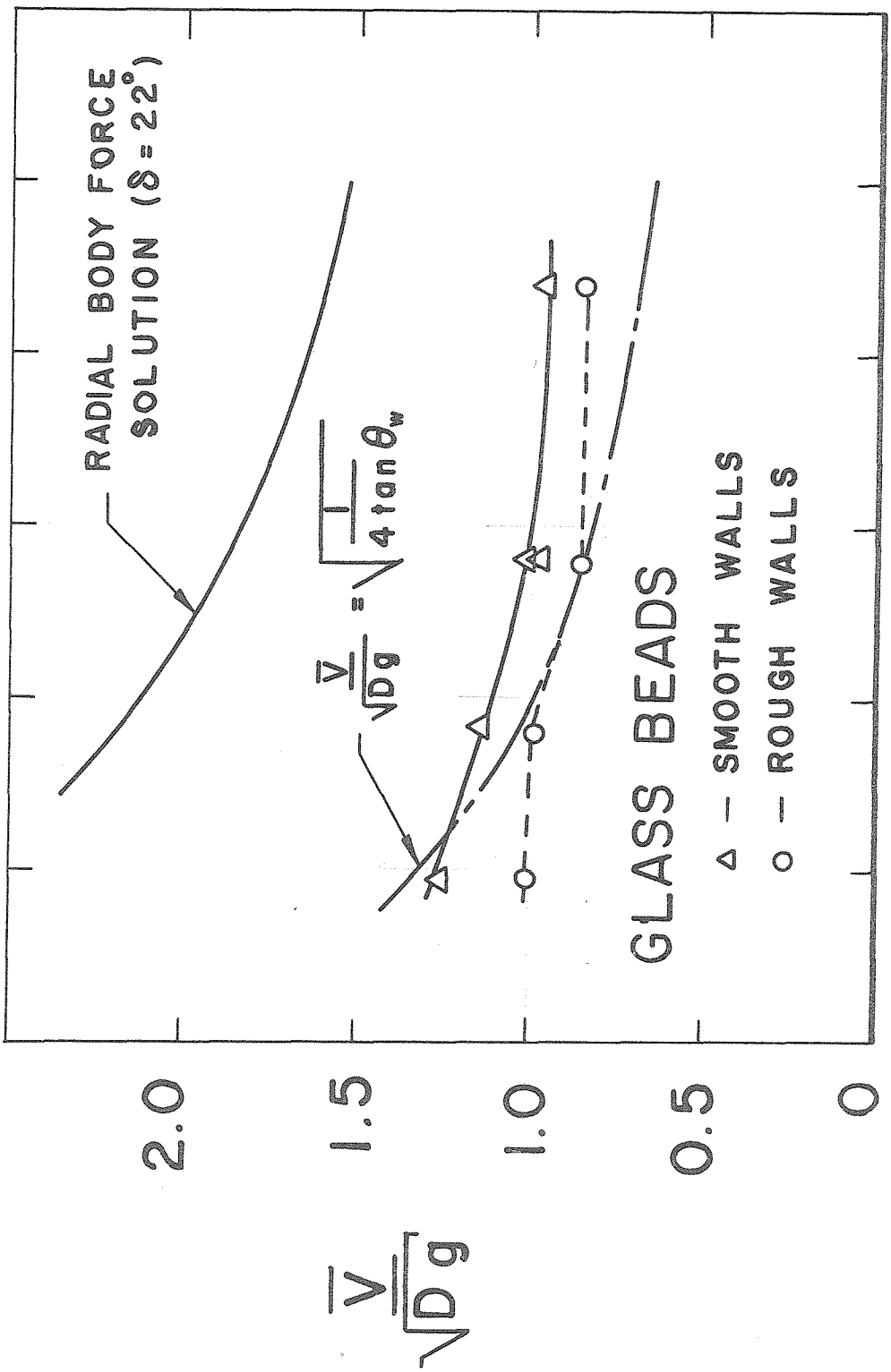

Figure 7 Dimensionless efflux velocity for glass beads ($\delta = 22°$) flowing through conical channels.

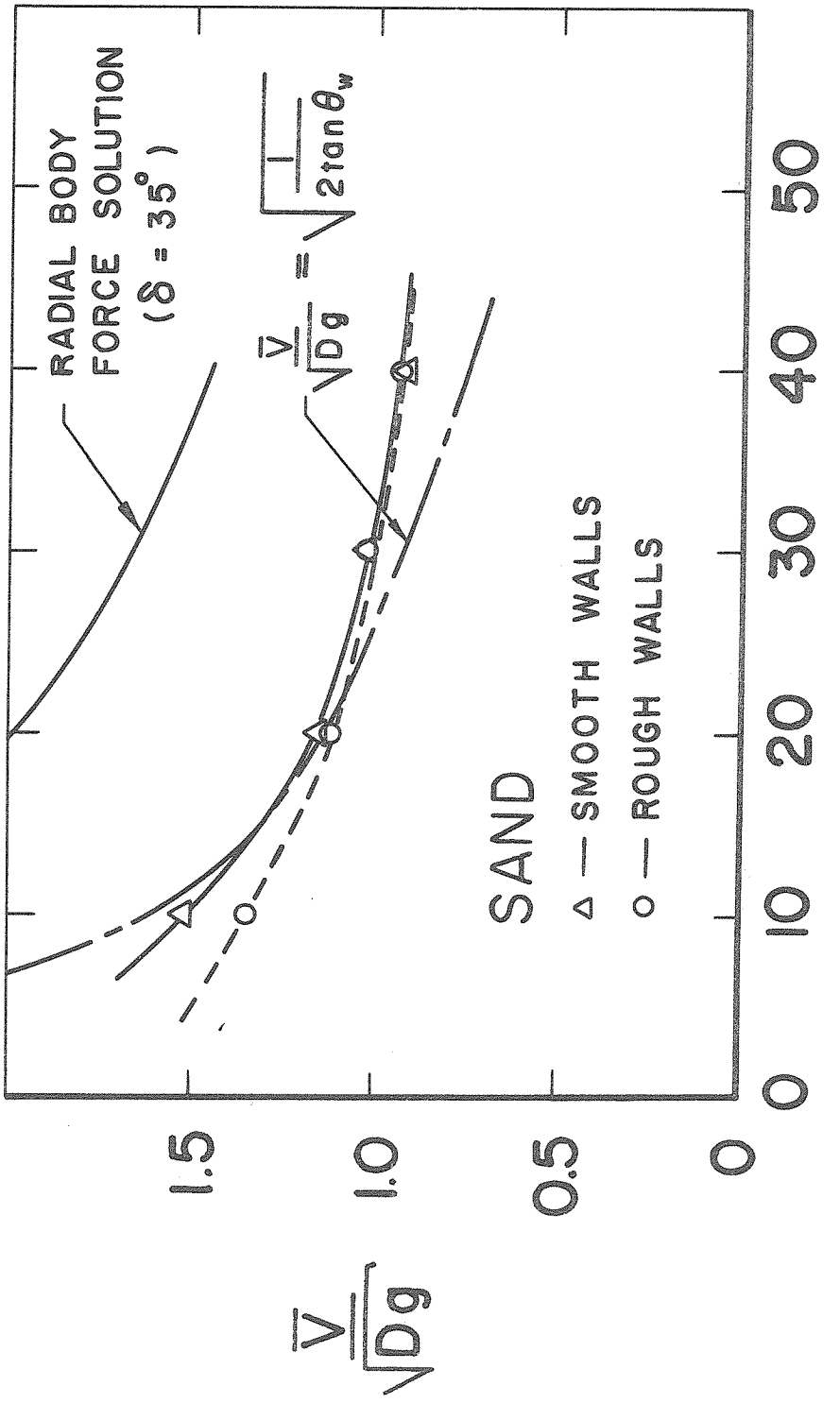

Figure 8 Dimensionless efflux velocity for sand ($\delta = 35°$) flowing through plane channels.

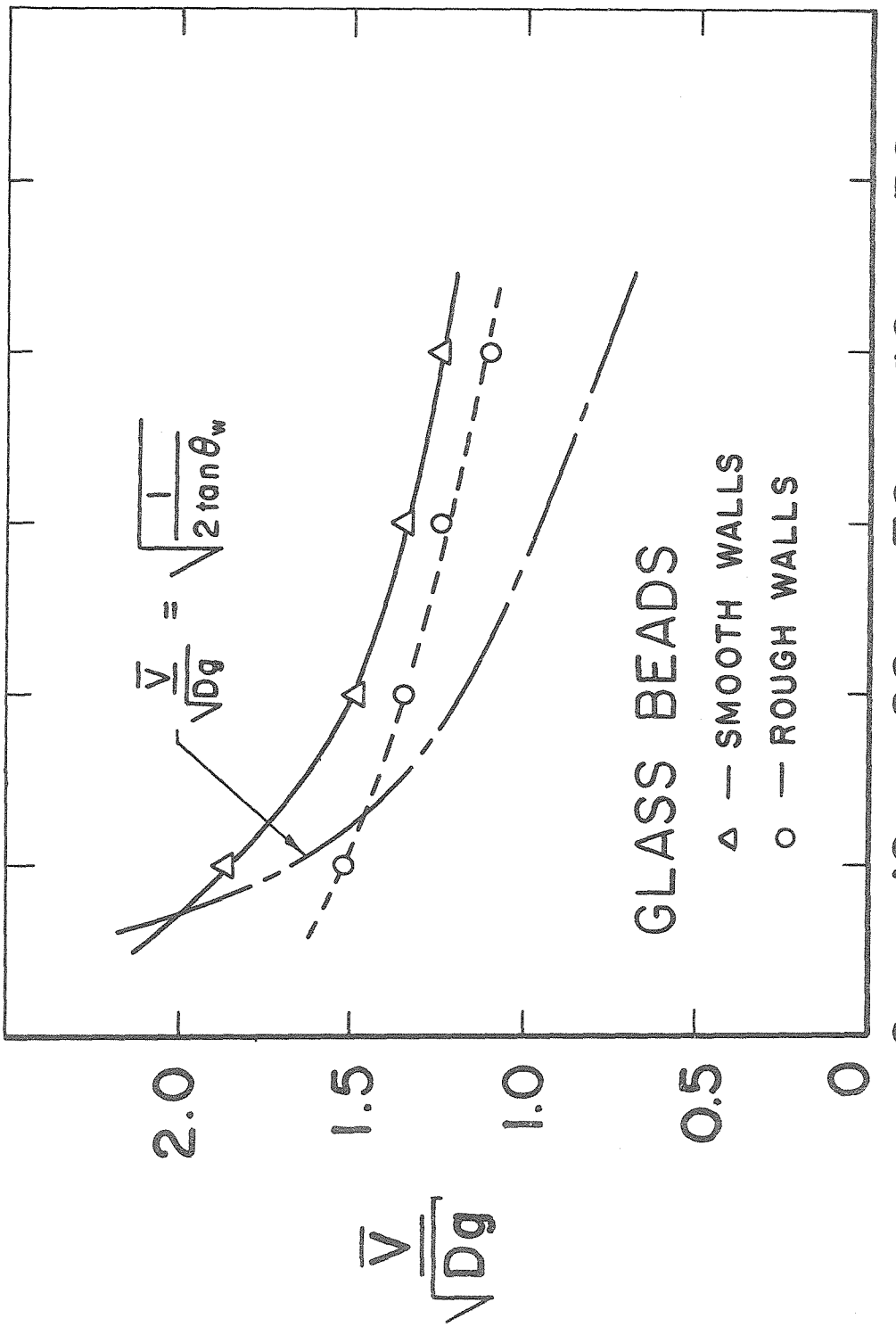

Figure 9 Dimensionless efflux velocity for glass beads ($\delta = 22°$) flowing through plane channels.

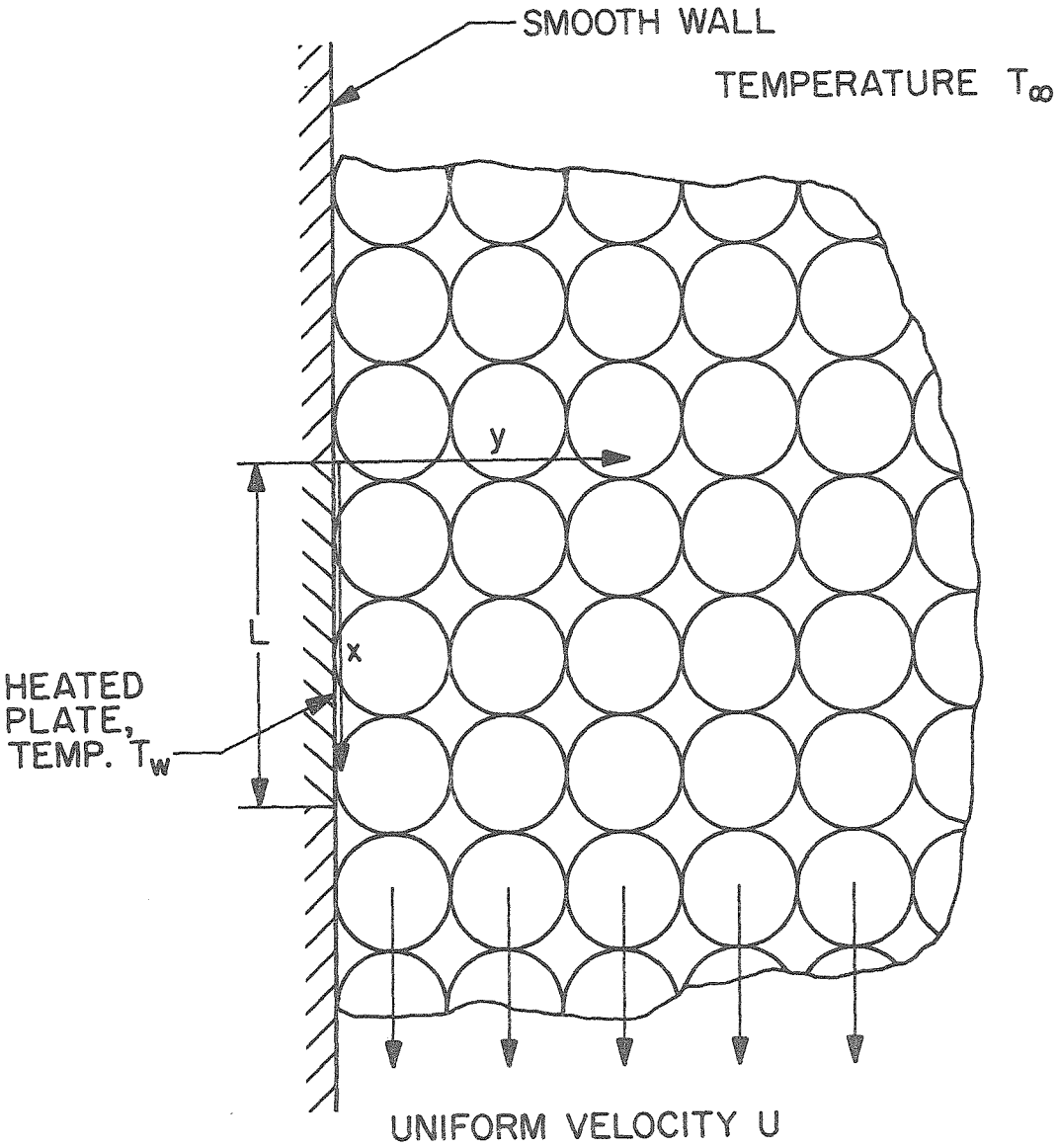

Figure 10 Discrete particle flow past a heated plate.

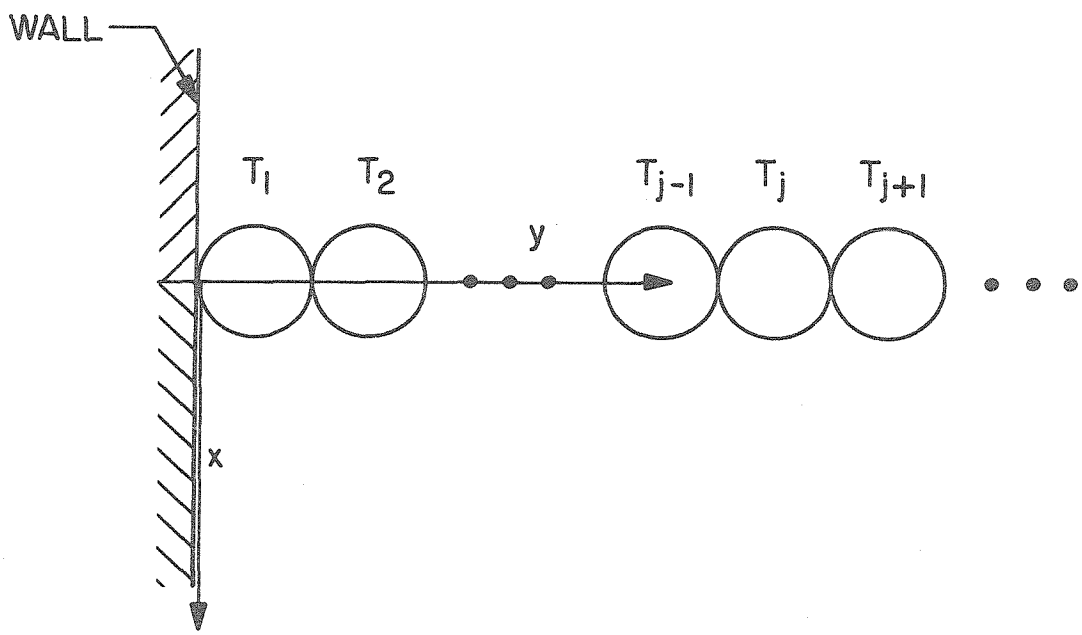

Figure 11 Typical row of particles in a discrete particle flow.

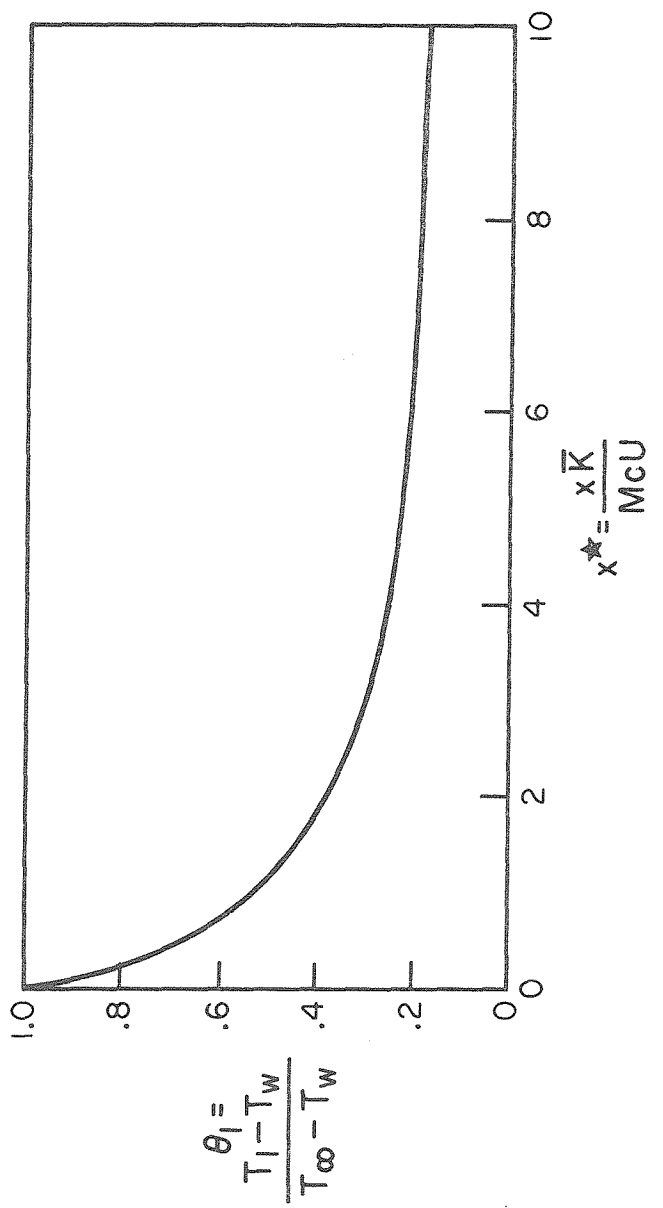

Figure 12 Dimensionless temperature of the first particle, $\theta_1(x^*)$, for a constant temperature plate.

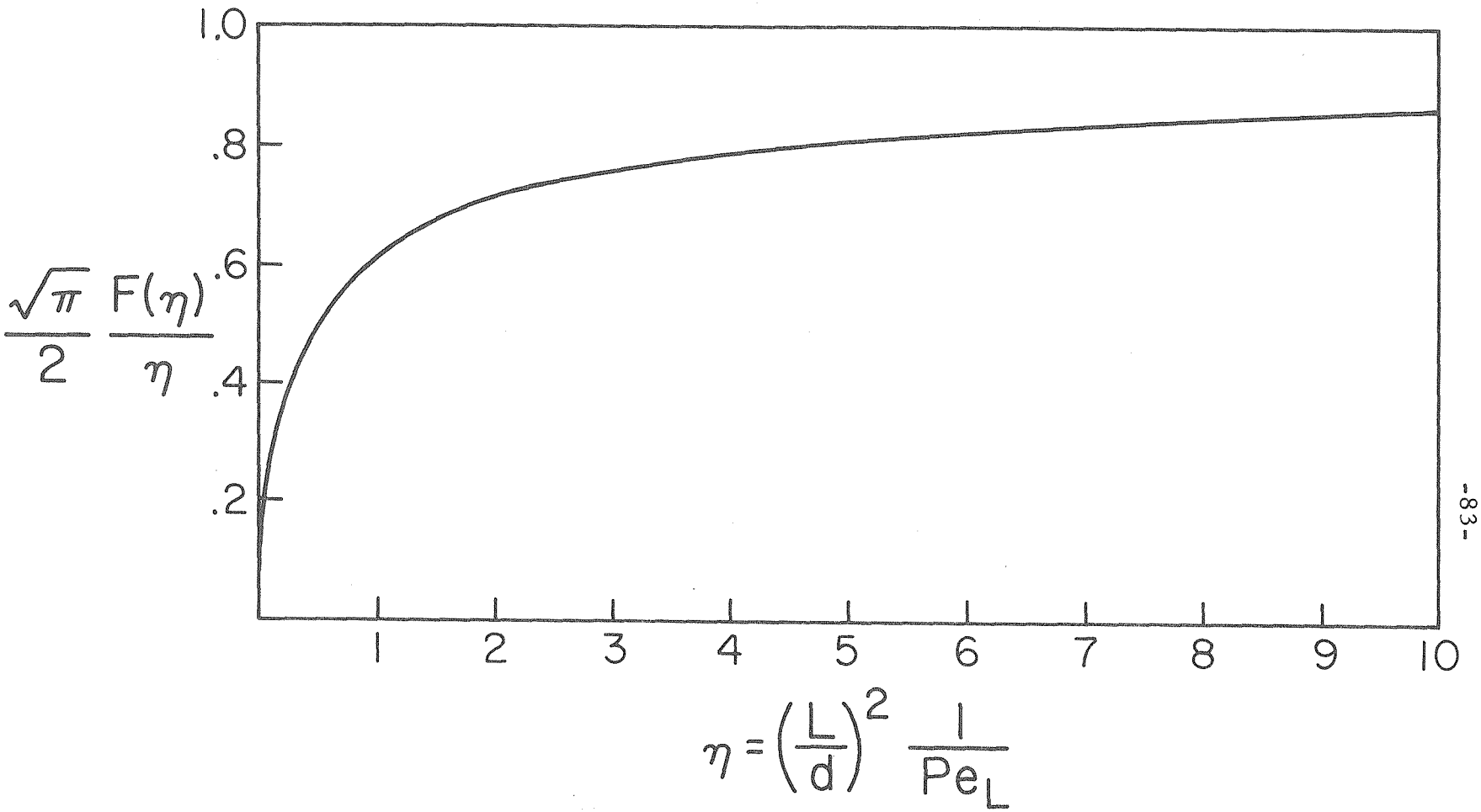

Figure 13 Comparison of heat transfer for the discrete particles and a one-component continuum.

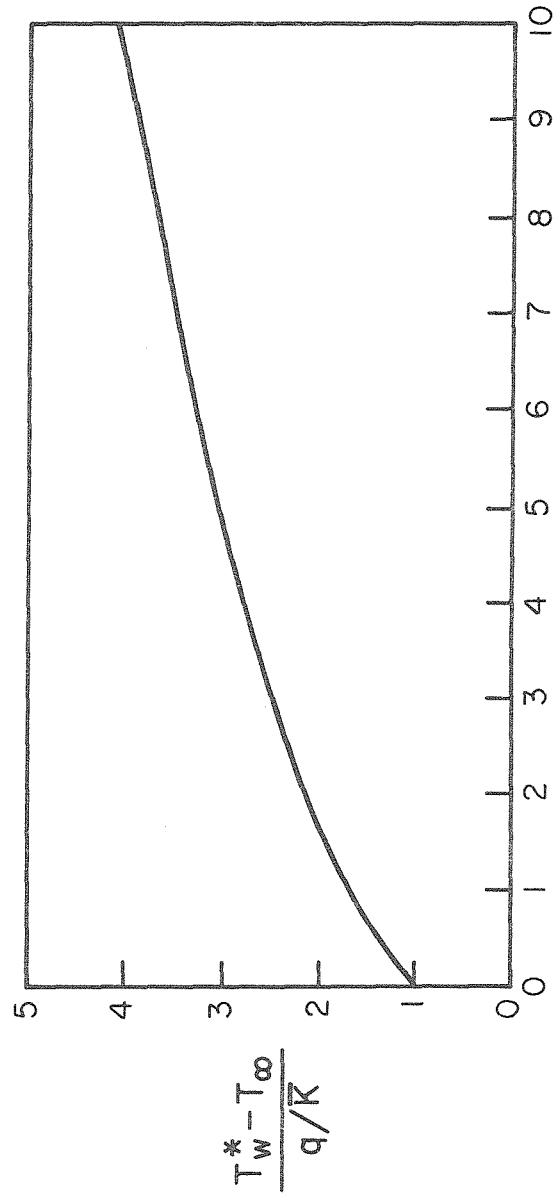

Figure 14 Dimensionless wall temperature distribution for a constant heat flux plate.

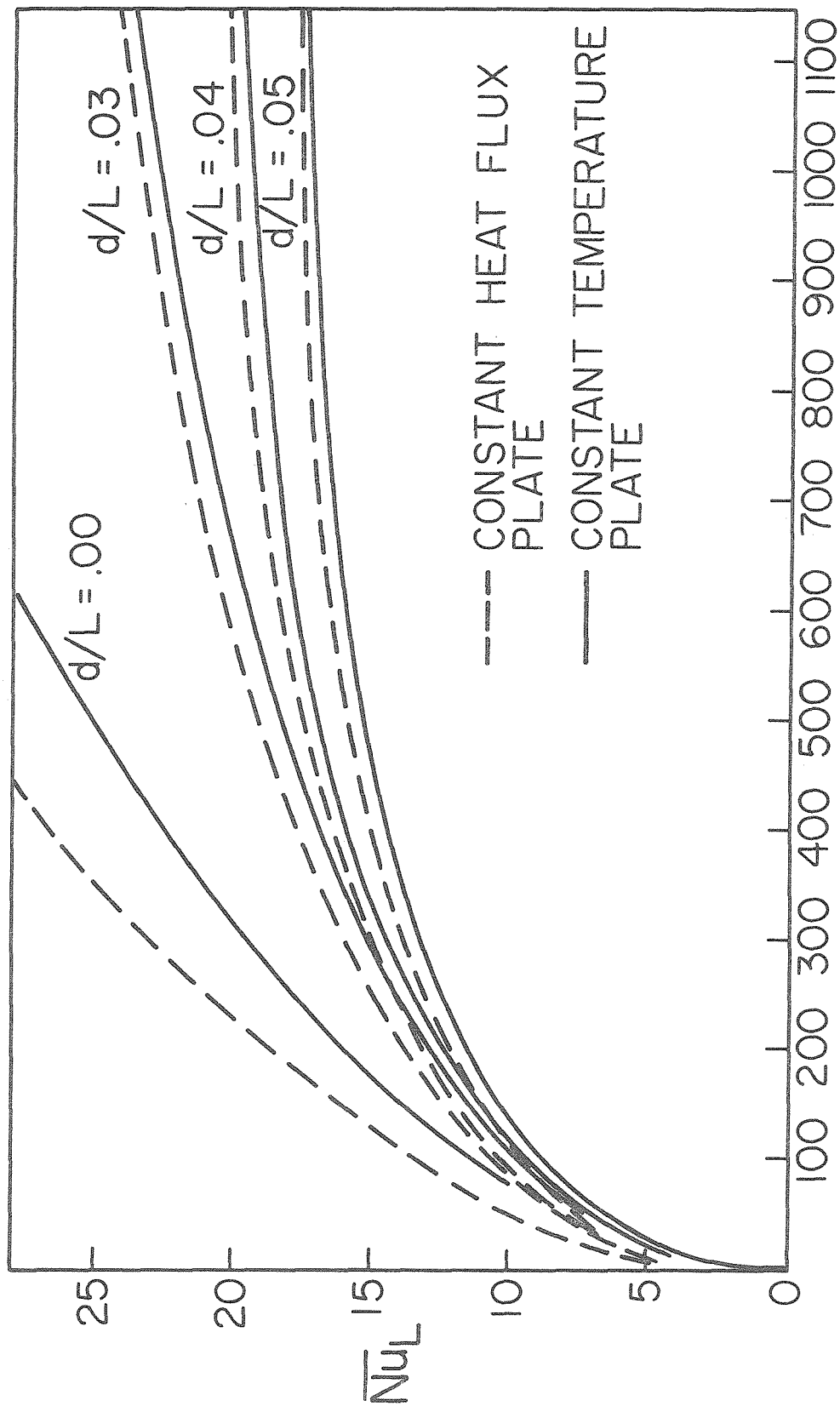

Figure 15 Average Nusselt number as a function of Péclét number for the discrete particle model.

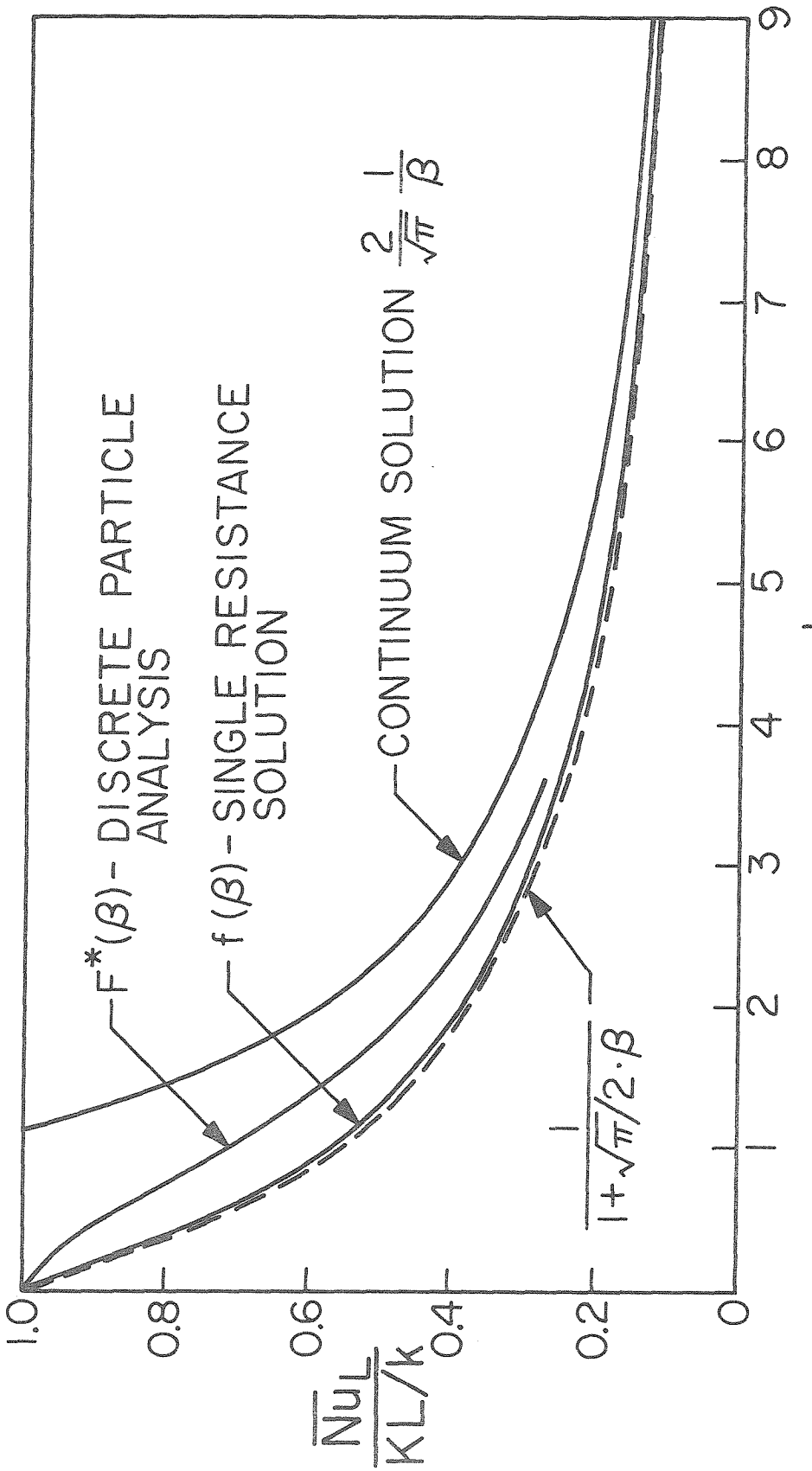

Figure 16 Comparison of the discrete particle solution with a continuum with conductance K at the plate surface, for a constant temperature plate.

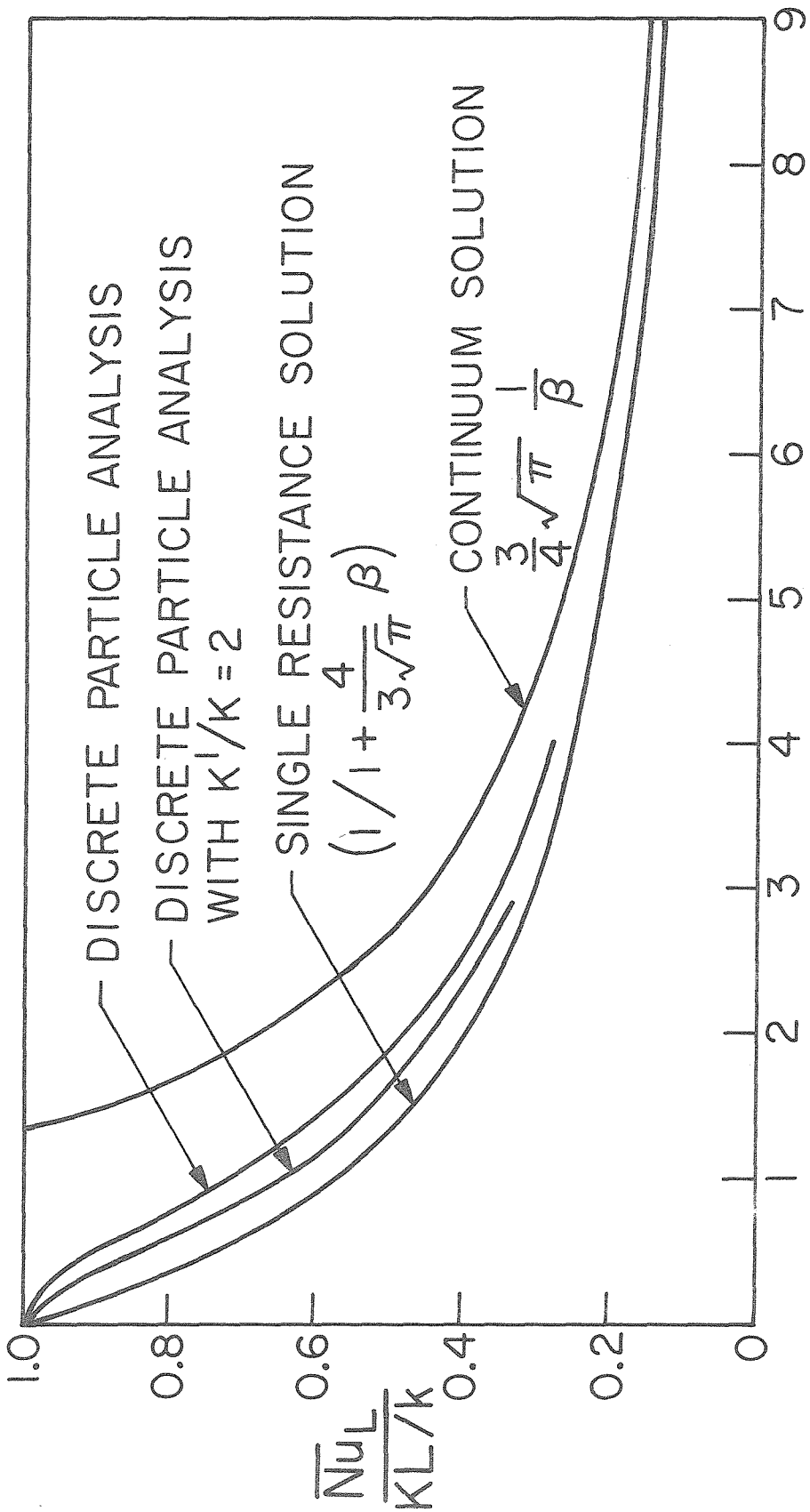

Figure 17 Comparison of the discrete particle solution with a continuum with conductance K at the plate surface, for a constant heat flux plate.

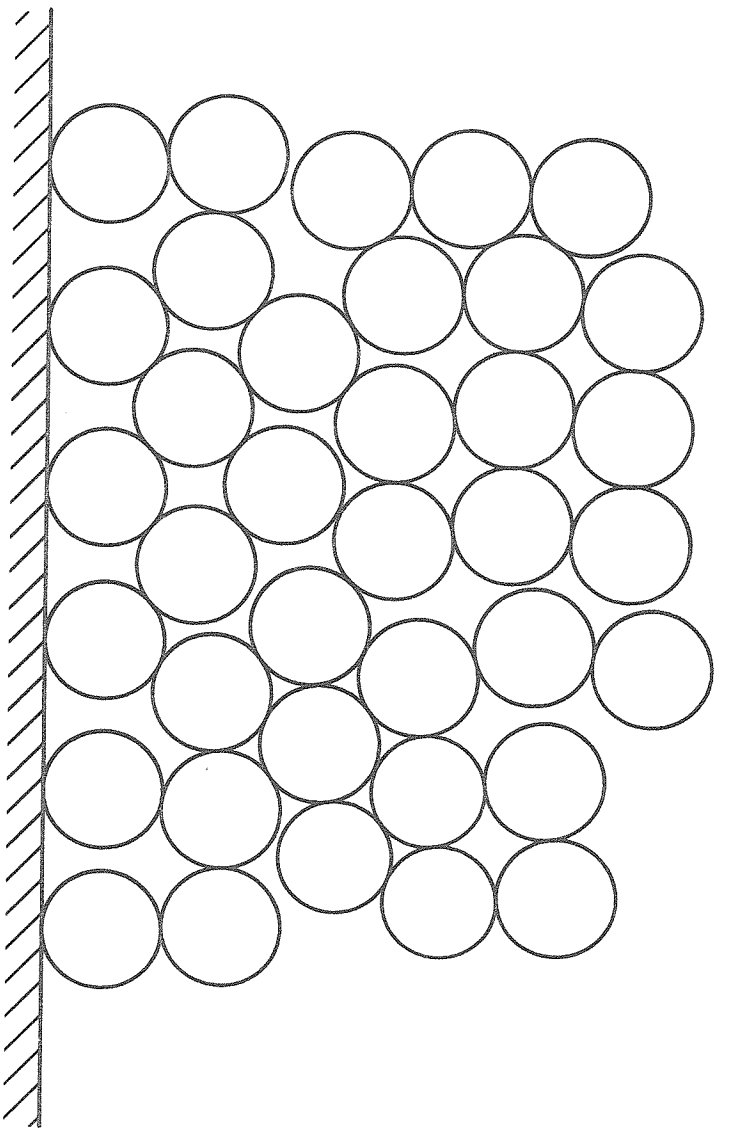

Figure 18 Typical particle arrangement in an actual flow, with increased voidage near the wall.

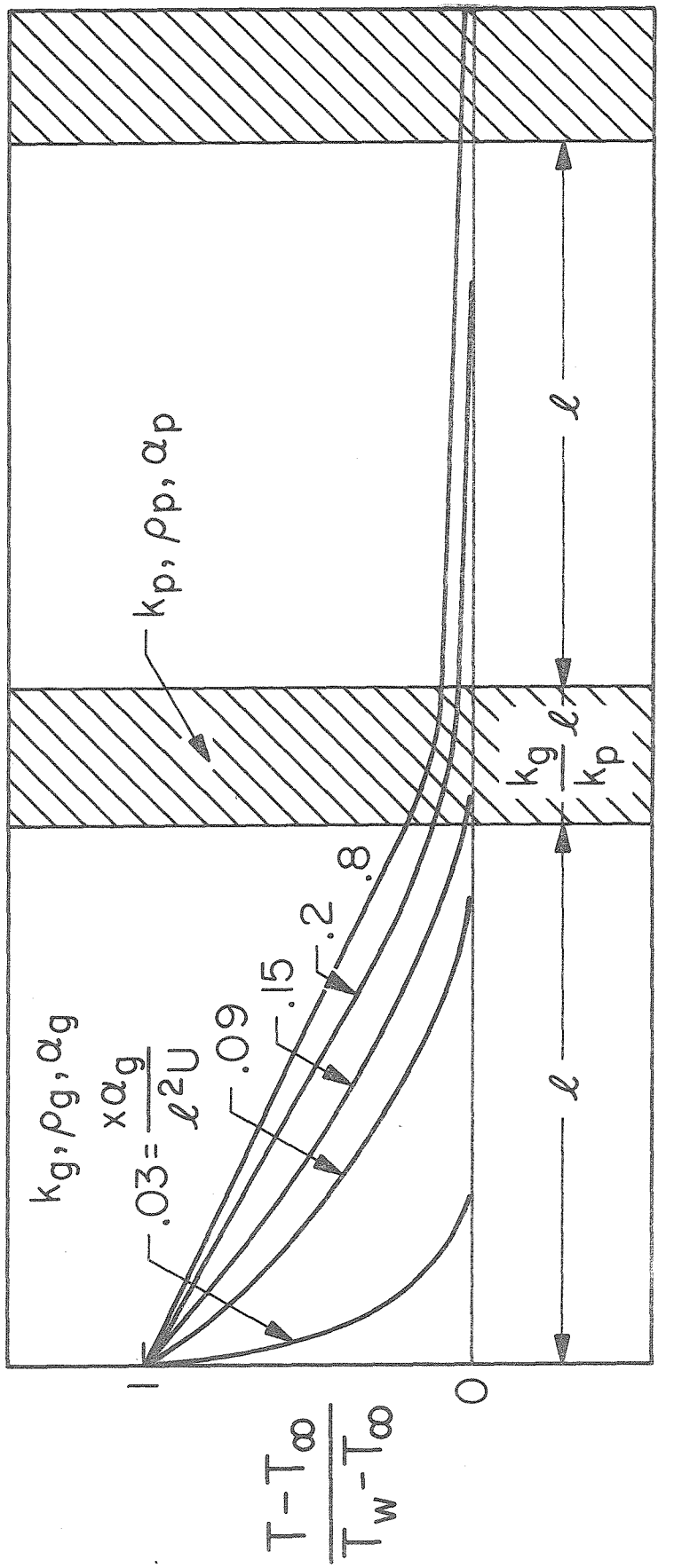

Figure 19 Schmidt plot results for the temperature distribution in a laminated medium, with $k_p \rho_p c_p / k_g \rho_g c_g$ equal to 4.

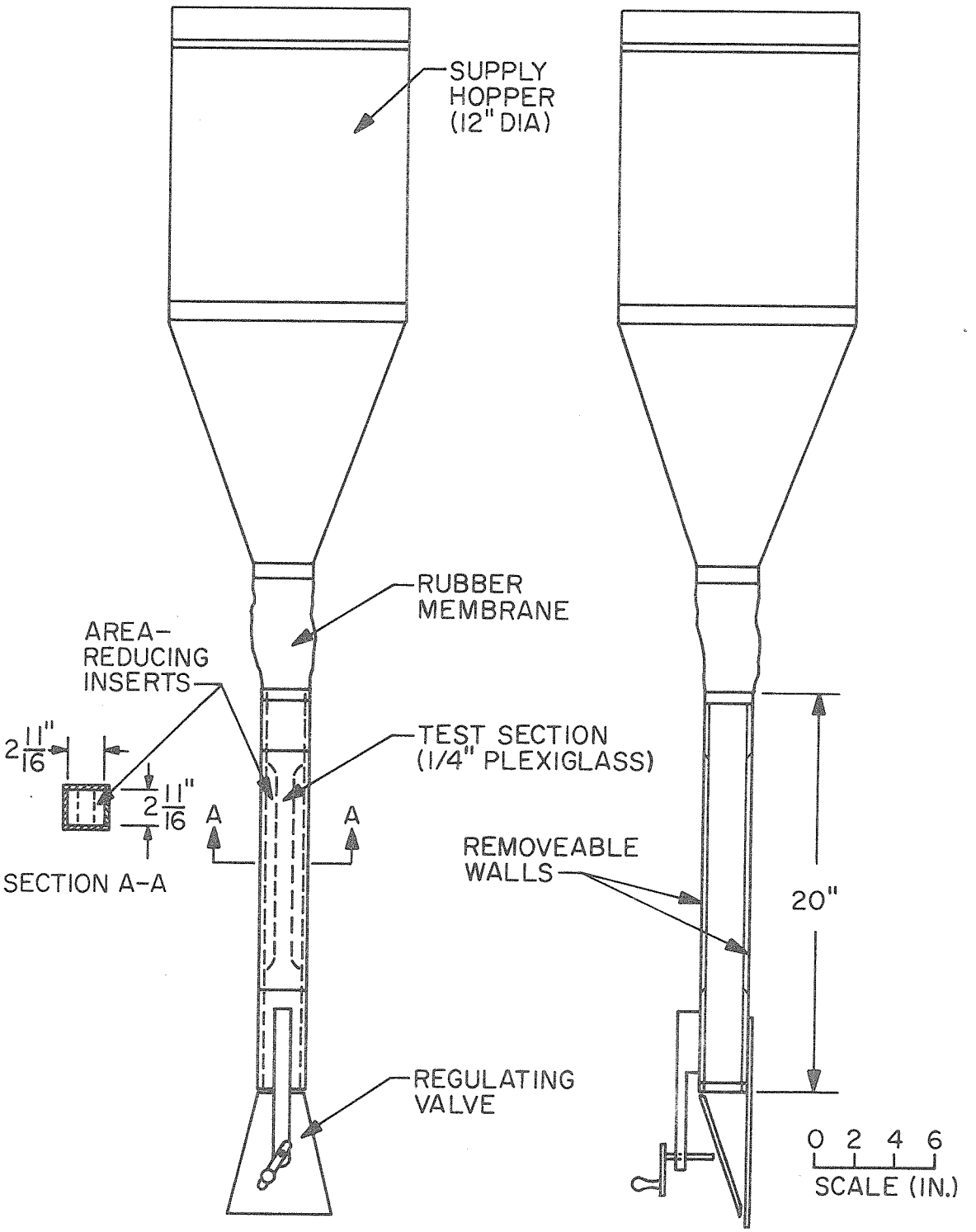

Figure 20 Schematic diagram of the flow apparatus.

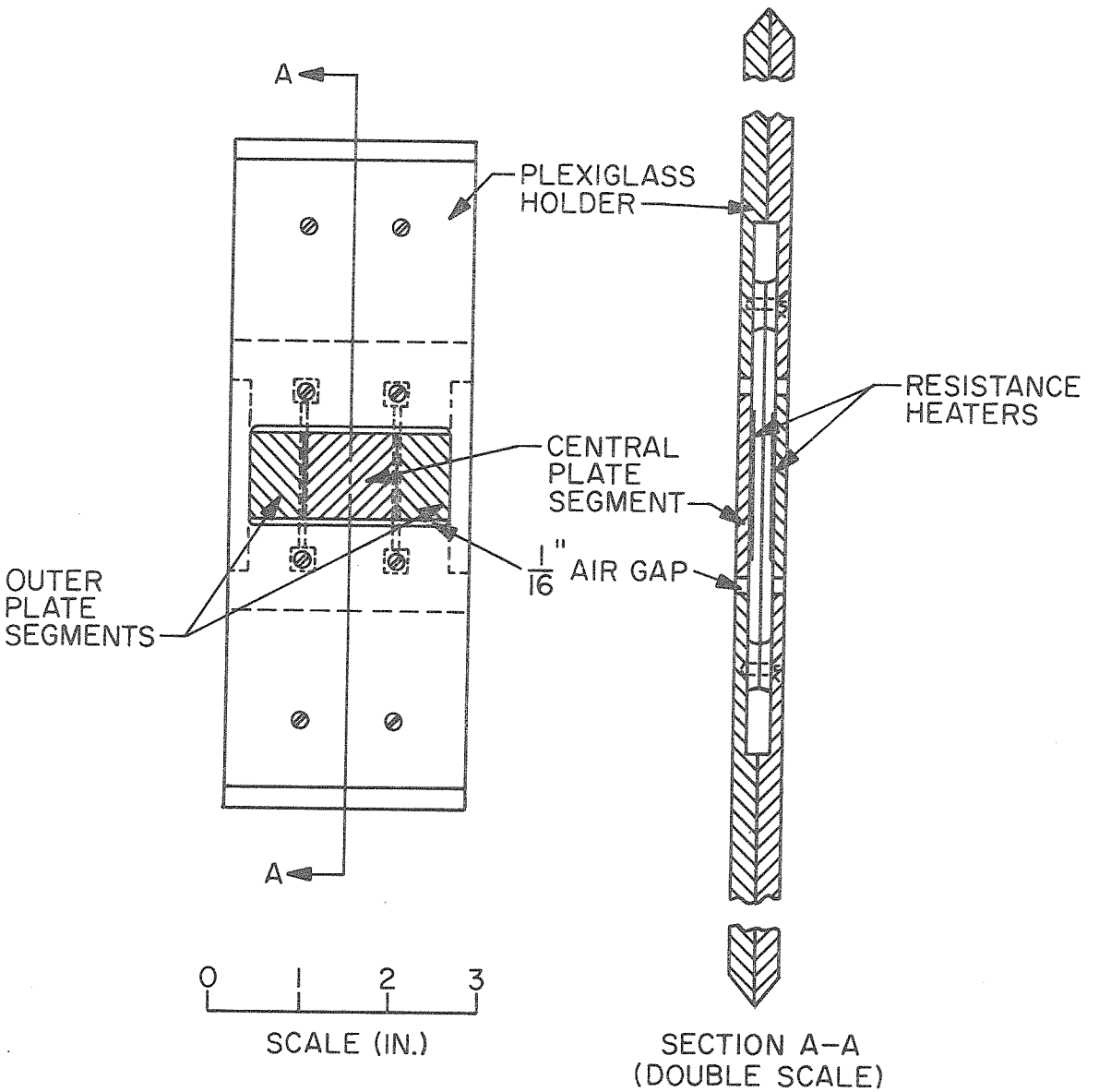

Figure 21 Schematic diagram of the flat plate model.

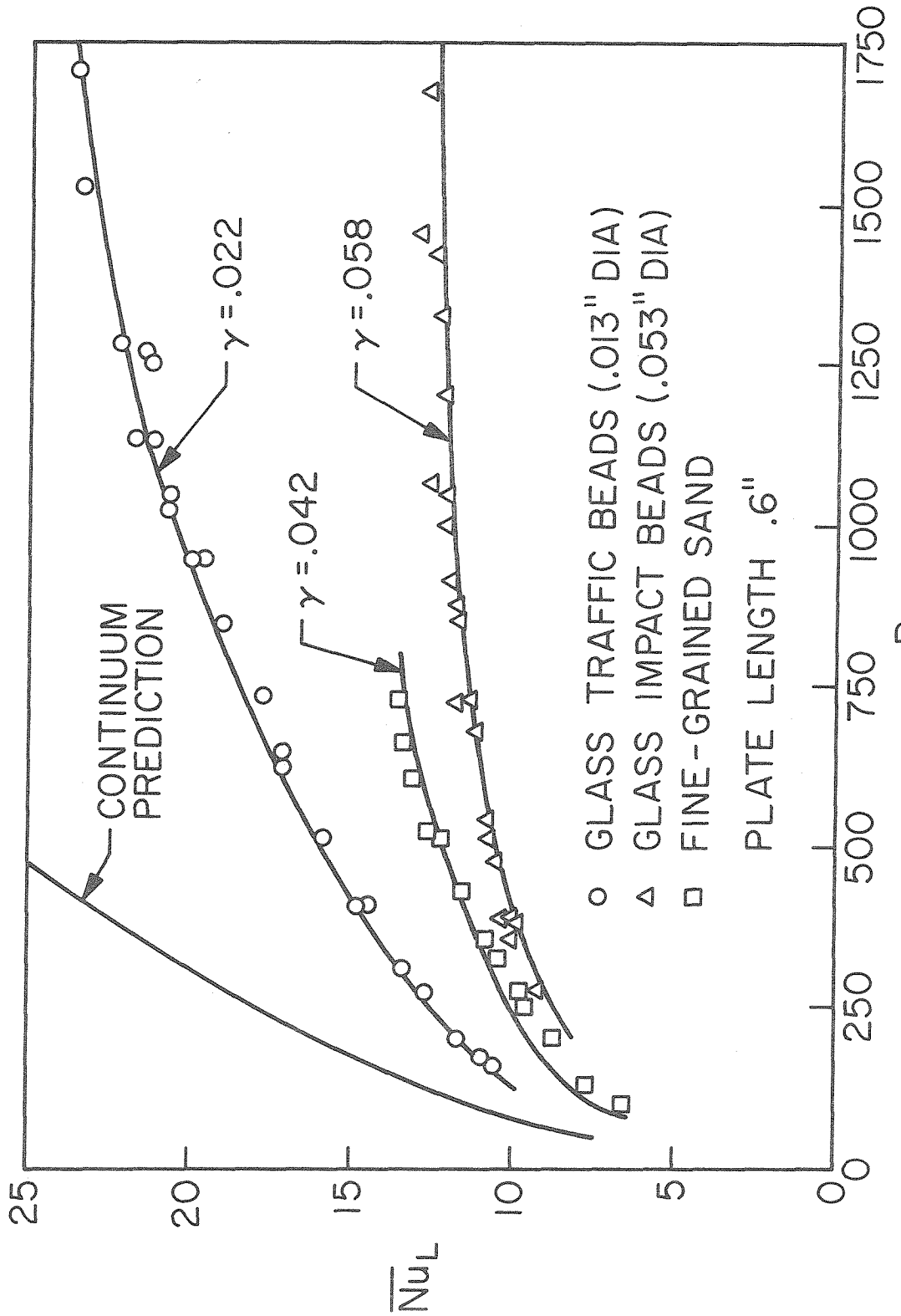

Figure 22 Nusselt number versus Péclét number data for the .6" plate.

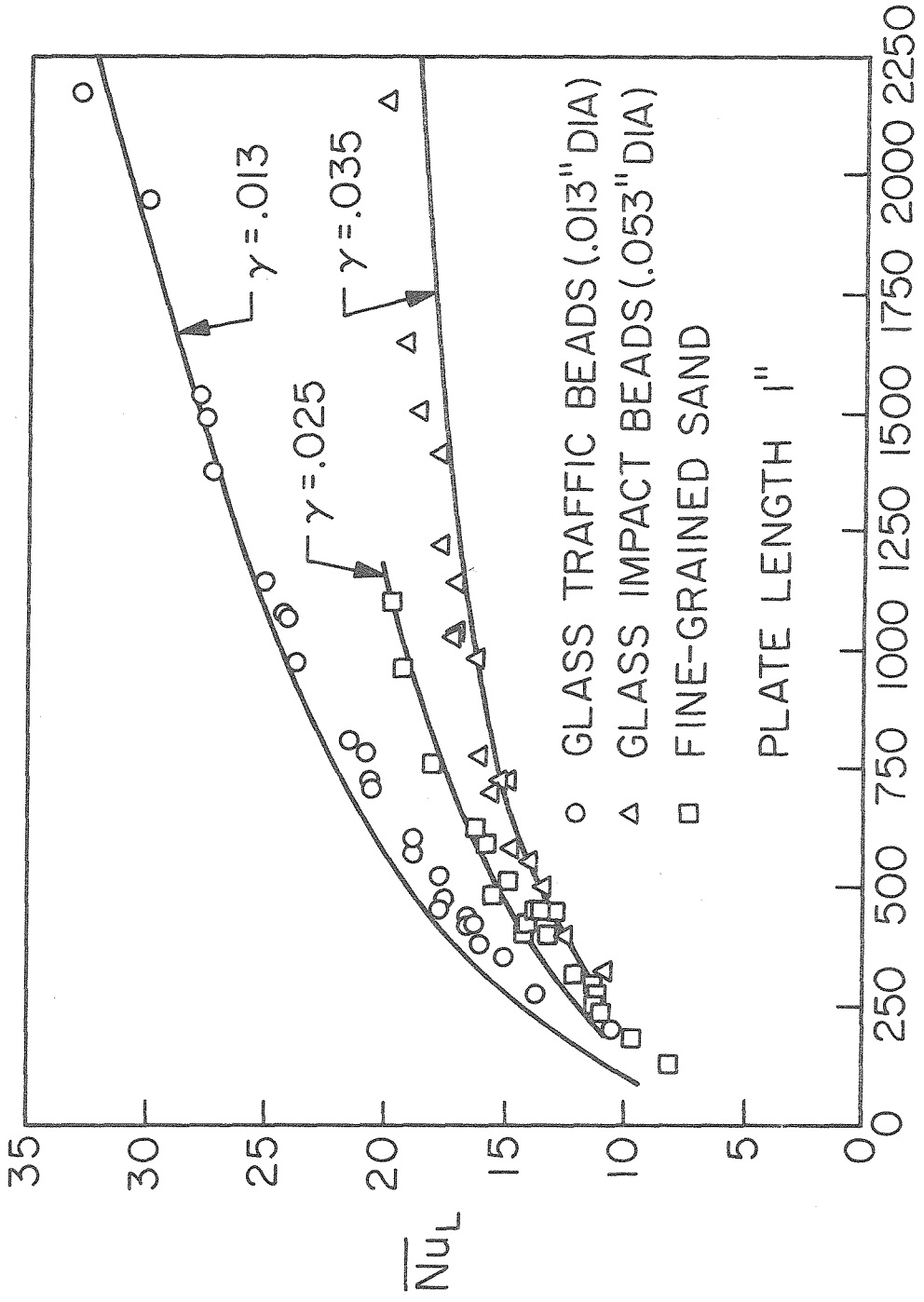

Figure 23 Nusselt number versus Péclét number data for the 1" plate.

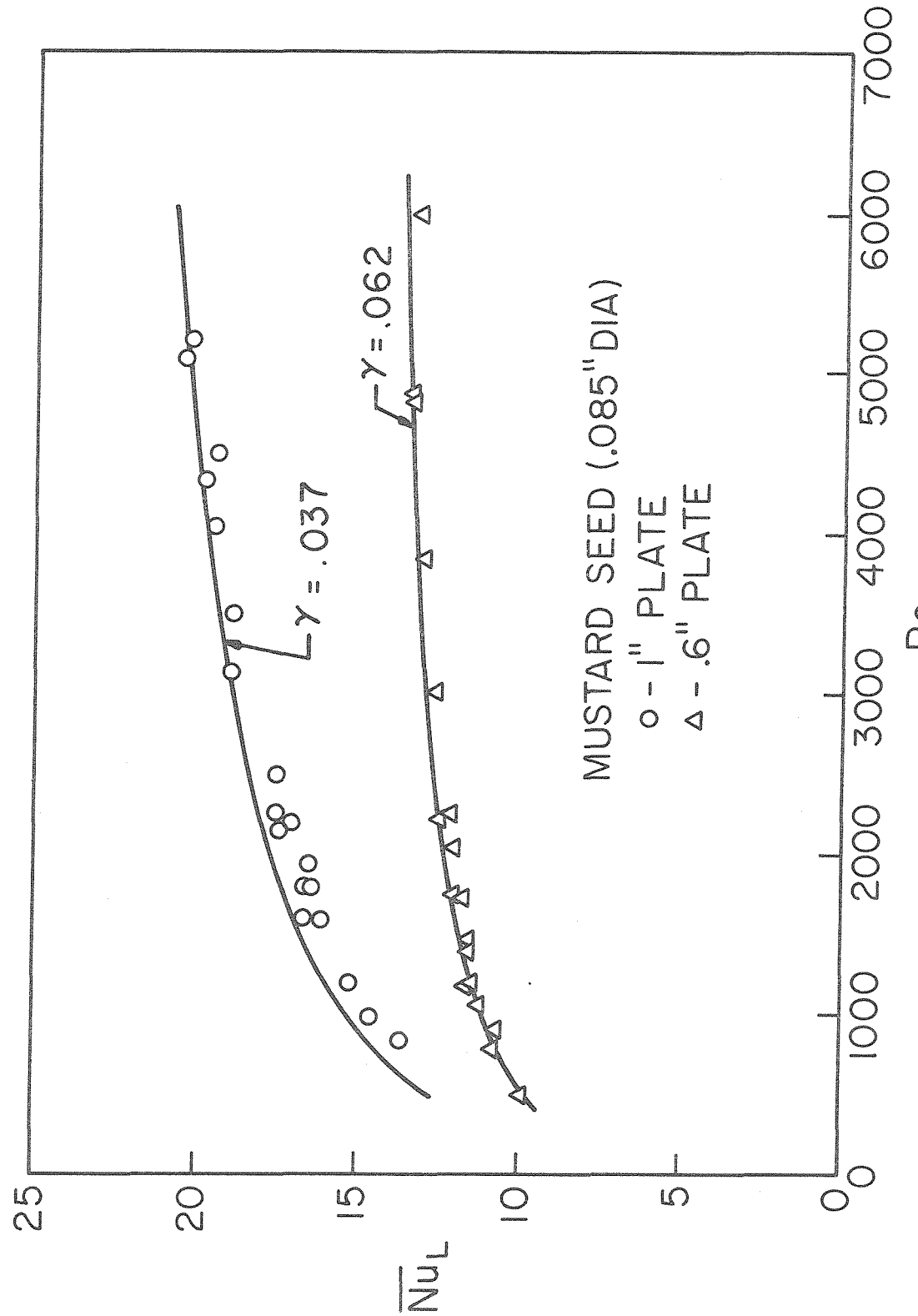

Figure 24 Nusselt number versus Péclét number data for the mustard seed, using the .6" and 1" plate.

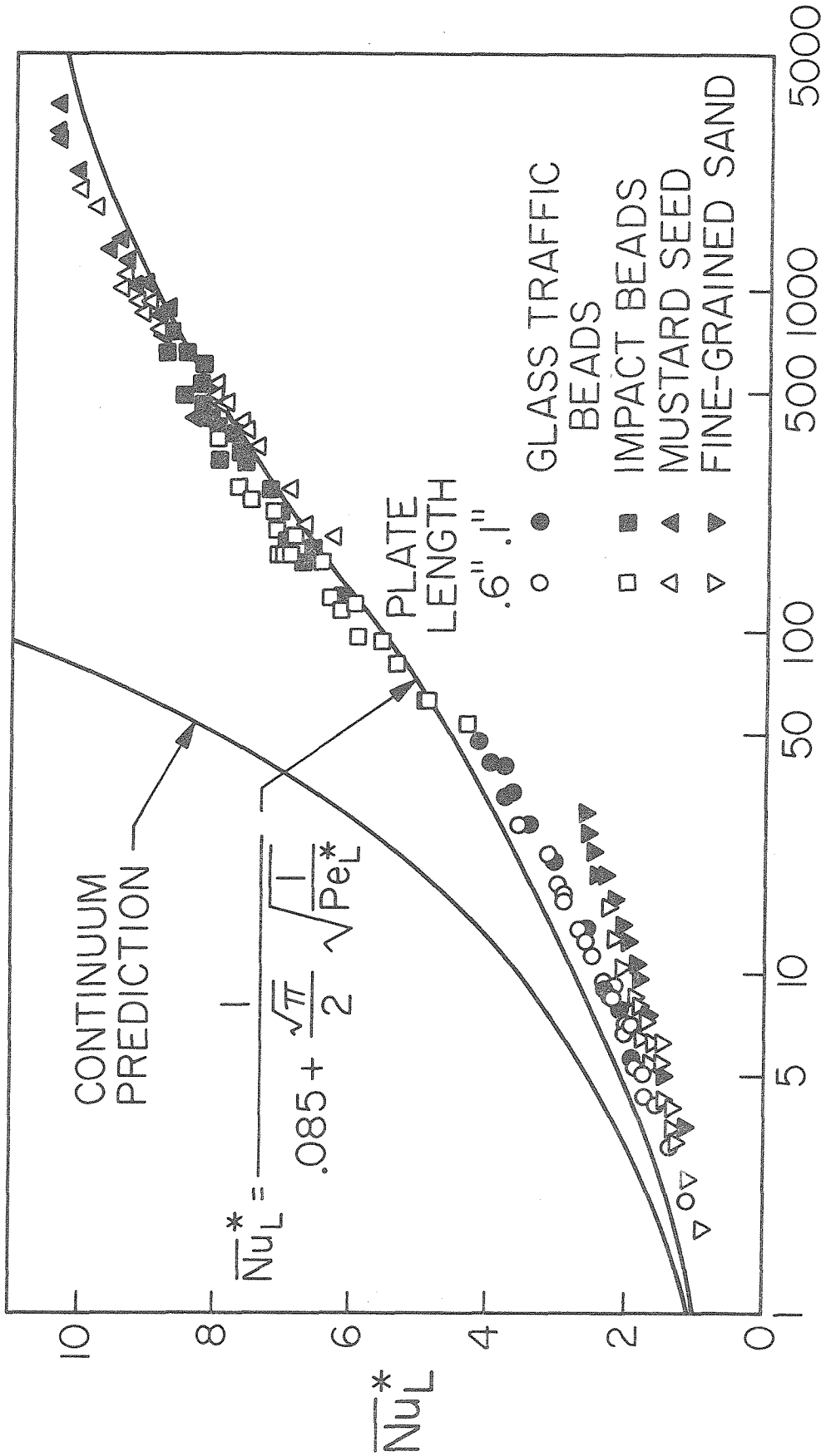

Figure 25 Modified Nusselt number versus modified Péclét number data for all materials tested, with both plate lengths.

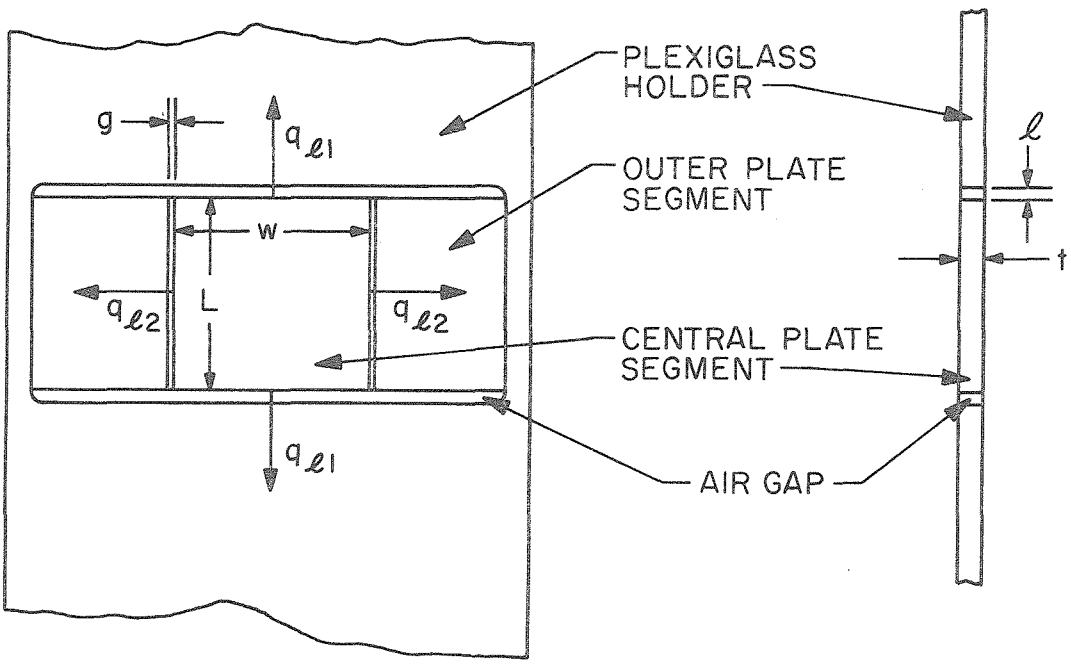

L =	.6", 1"
w =	1"
ℓ =	$\frac{1}{16}$"
t =	$\frac{1}{16}$"
g ≈	.002

Figure A-1 Central plate segment schematic indicating heat losses.

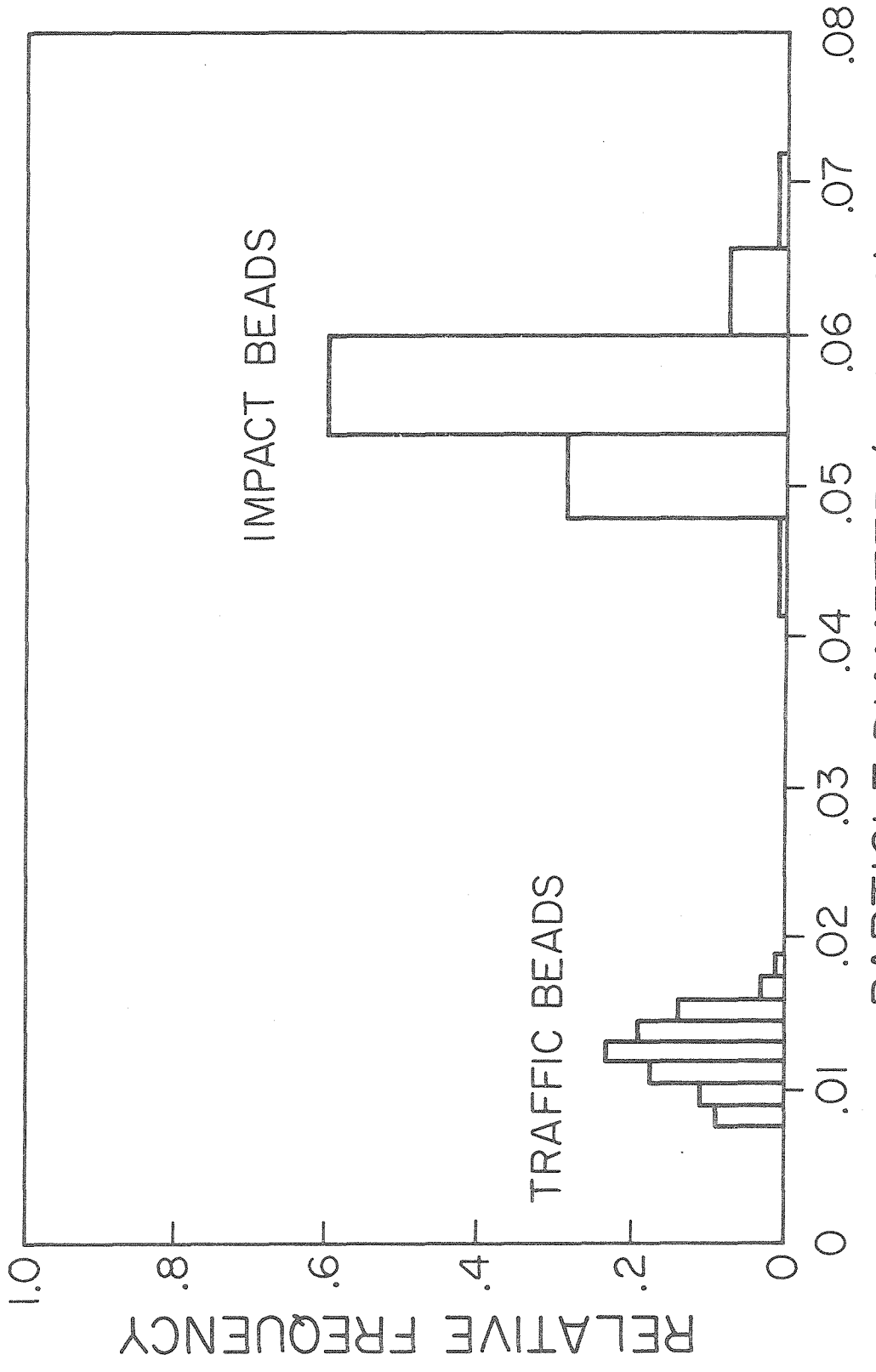

Figure B-1 Particle size histograms for glass traffic beads and glass impact beads.

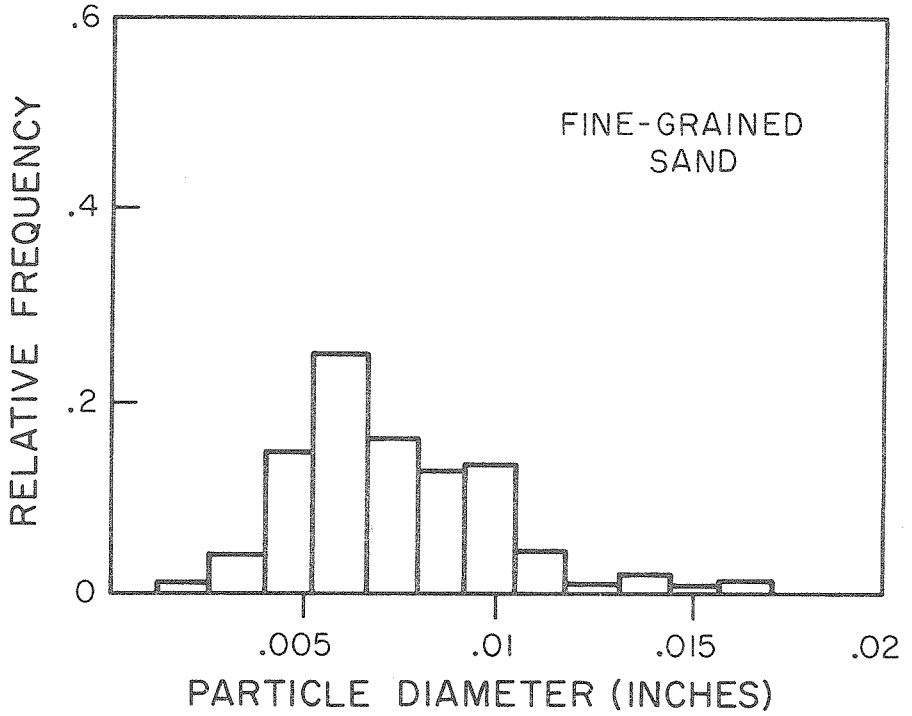

Figure B-2 Particle size histogram for fine-grained sand.

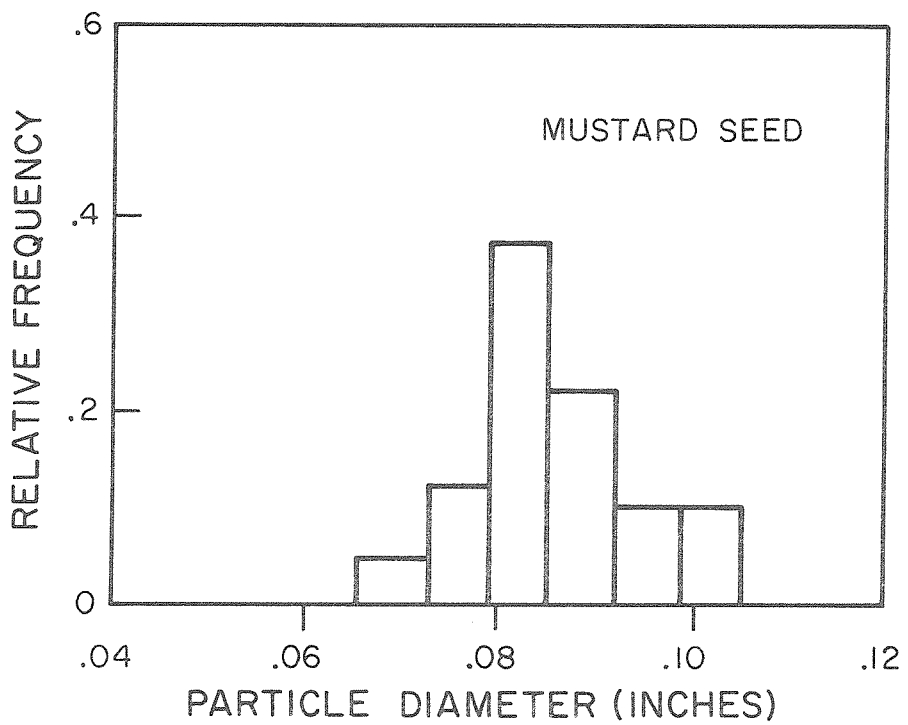

Figure B-3 Particle size histogram for mustard seed.

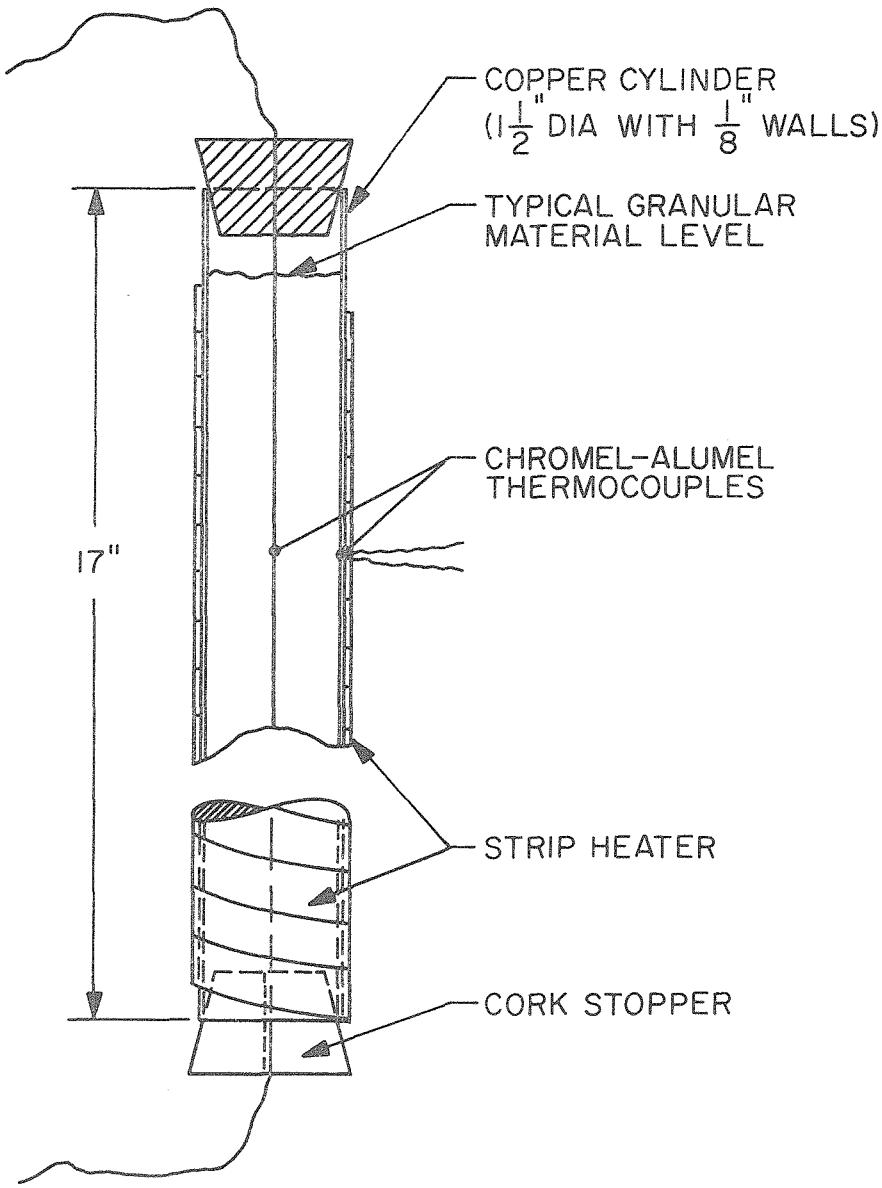

Figure B-4 Schematic diagram of apparatus used for diffusivity measurements.

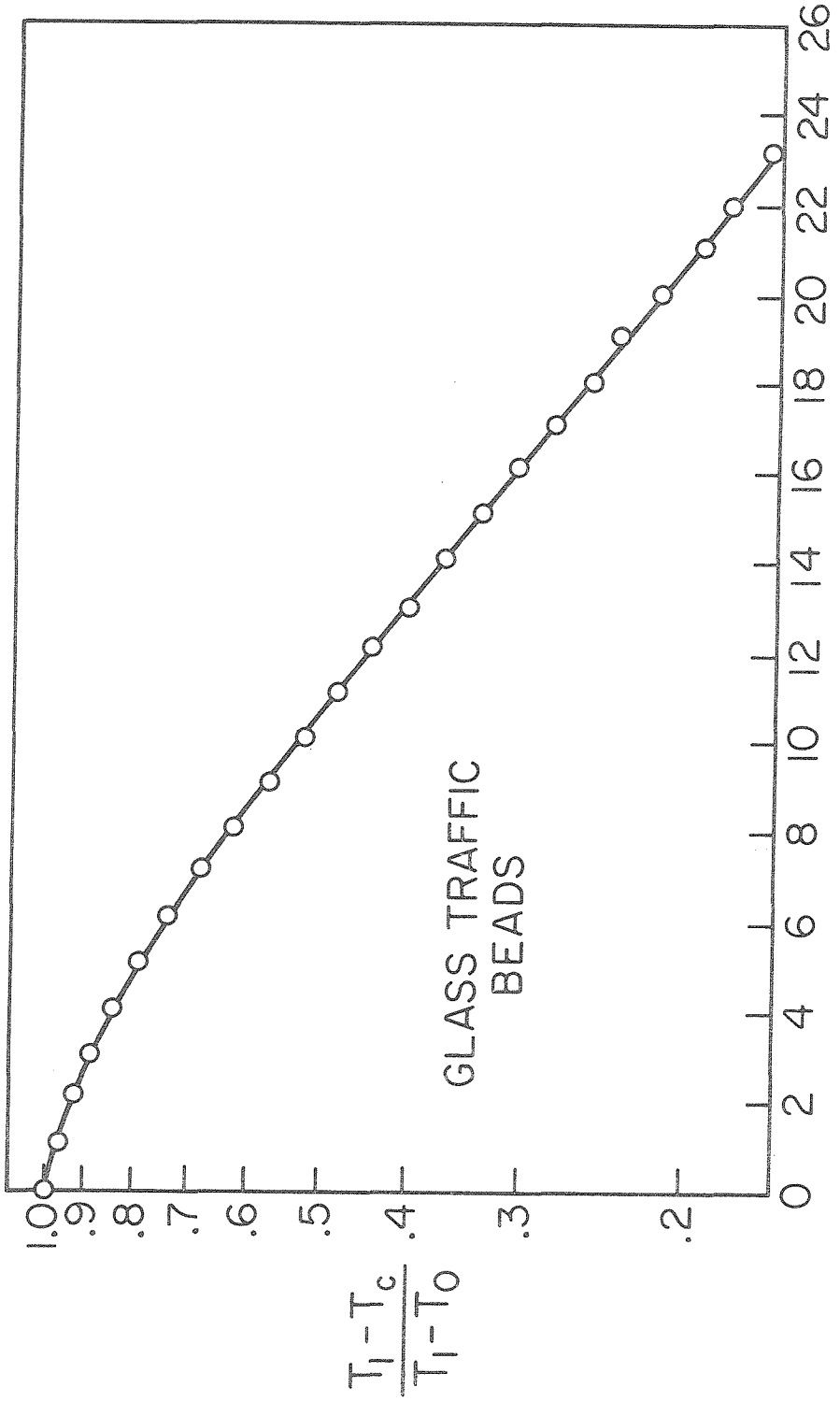

Figure B-5 Typical temperature-time plot for the diffusivity experiment.

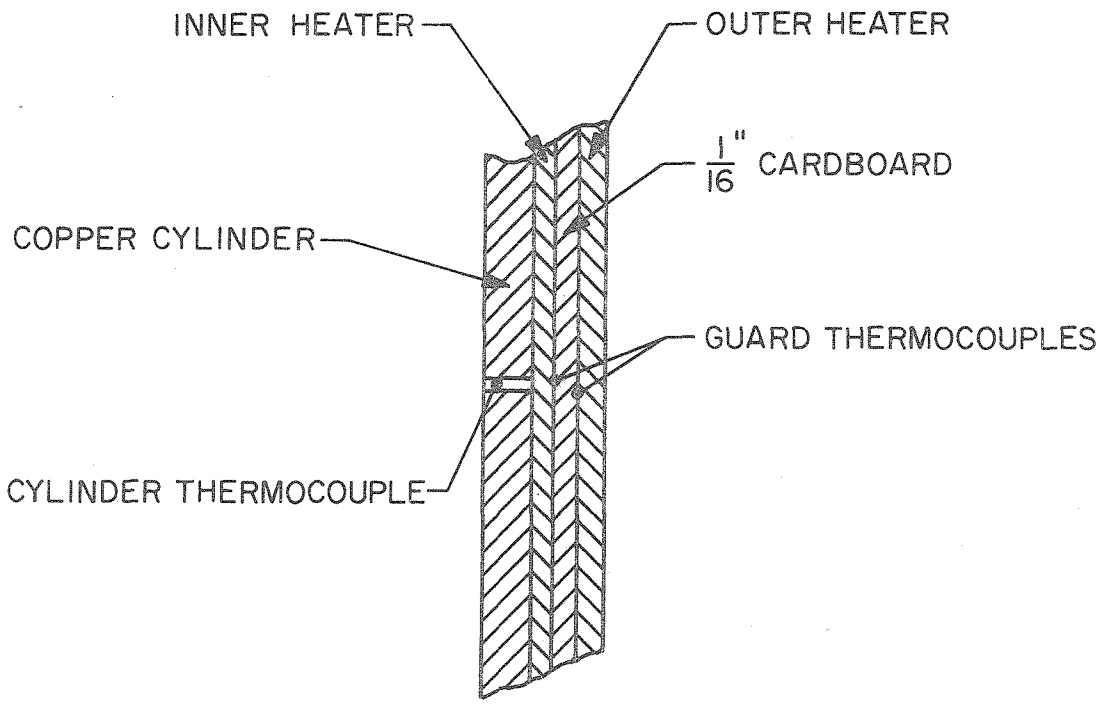

Figure B-6 Section of the cylinder wall as modified for the specific heat measurement.

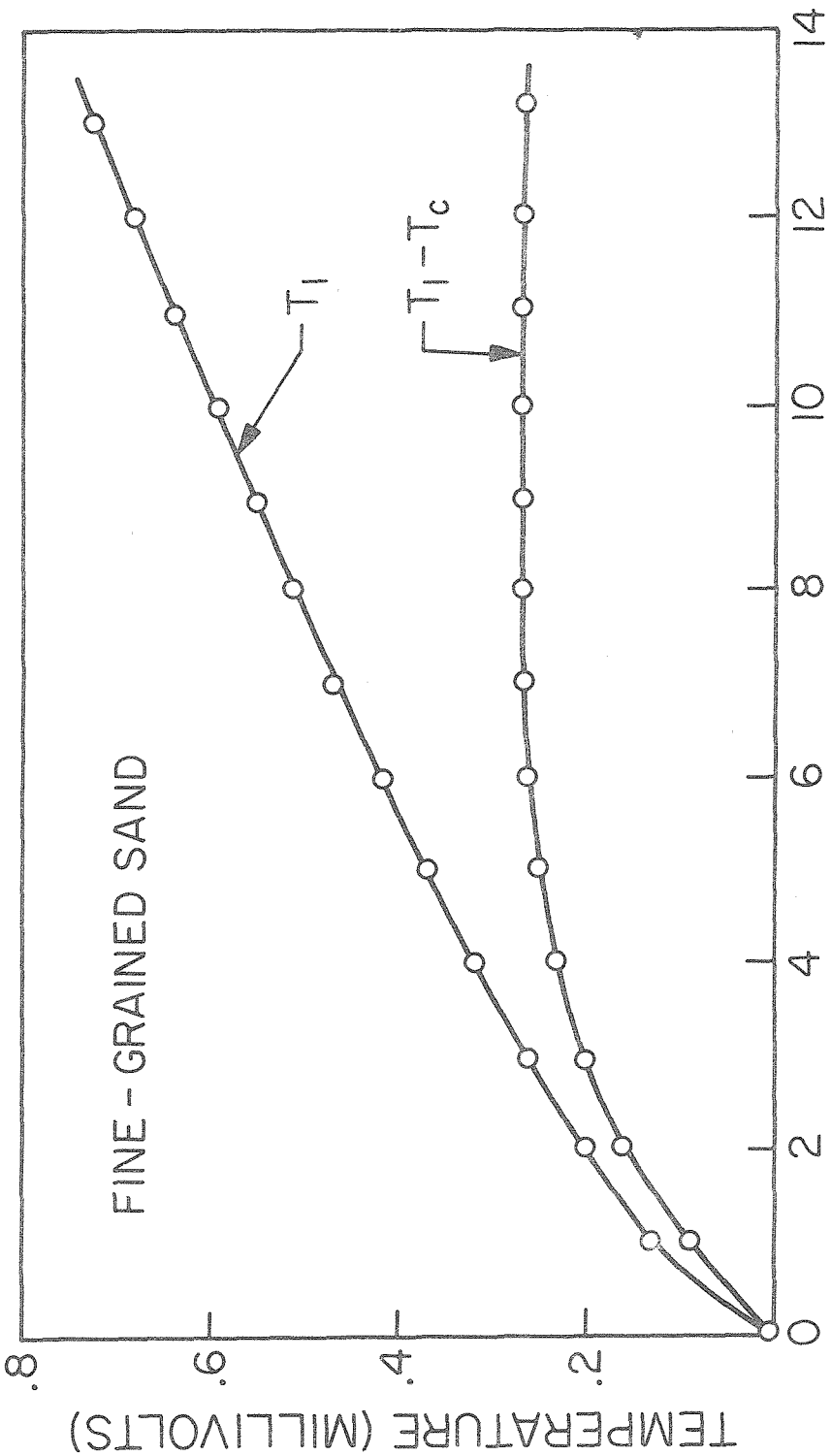

Figure B-7 Typical temperature-time plot for the specific heat experiment.